Geotech Geol Eng (2026) 44:305
https://doi.org/10.1007/s10706-026-03824-0

ORIGINAL PAPER

Stochastic Polynomial Surrogate Models for Uncertainty Quantification of Offshore Plate Anchor Capacity

Negin Yousefpour · Bo Wang · Changjian Zhou · Alessio Mentani

Received: 10 March 2026 / Accepted: 16 July 2026 / Published online: 21 July 2026

Abstract Uncertainty quantification (UQ) is essential for the reliable design of offshore plate anchors, where prediction accuracy is influenced by uncertainties in model parameters, soil properties, loading conditions, and numerical modelling. This paper presents a unified UQ framework that integrates Bayesian inference with stochastic Polynomial Chaos Expansion (PCE) surrogate modelling to efficiently quantify multiple sources of uncertainty in plate anchor capacity under combined vertical–horizontal–moment (V–H–M) loading. While surrogate modelling techniques have been applied to selected offshore foundation problems, their application to comprehensive uncertainty quantification of plate anchors under combined loading remains limited. In particular, addressing model parameter, soil strength and loading uncertainties, as well as numerical approximation error effects within a single framework has not previously been investigated. The proposed UQ framework is demonstrated through a simplified plate anchor case study and comprises two complementary workflows: (1) Workflow A, this method integrates Bayesian calibration of an analytical yield-surface model with a PCE surrogate, providing a controlled validation of the PCE methodology prior to its deployment on finite element simulations. This method enables evaluation of the impacts of yield surface model parameter uncertainty, undrained shear strength uncertainty, and numerical approximation error (mesh discretisation) on the estimated anchor capacities; (2) Workflow B, this method applies PCE directly to replace the computationally expensive finite element simulation of plate anchor for efficient uncertainty quantification, particularly focusing on the effects of undrained shear strength and loading inclination uncertainty on the estimated anchor capacities. The PCE surrogates in both workflows achieved excellent predictive performance with RMSE between 0.5 to 2.1 kN/m for workflow A and less than 0.5 kN/m for workflow B, over both vertical and horizontal capacities, while significantly reducing computational cost. The results demonstrate that uncertainties in both soil strength and loading inclination led to significant uncertainty in the predicted anchor capacities. Also, mesh discretisation (numerical approximation error) influenced the inferred phenomenological yield-surface parameters and introduced considerable uncertainty into the

Supplementary Information The online version contains supplementary material available at https://doi.org/10.1007/s10706-026-03824-0.

N. Yousefpour (✉) · B. Wang · C. Zhou
Department of Infrastructure Engineering, The University of Melbourne, Parkville, VIC 3010, Australia
e-mail: negin.yousefpour@unimelb.edu.au

Bo. Wang
e-mail: bo.wang@unimelb.edu.au

C. Zhou
e-mail: changjianz@student.unimelb.edu.au

A. Mentani
DICAM, University of Bologna, 40100 Bologna, Italy
e-mail: alessio.mentani2@unibo.it

estimated anchor capacities. Although demonstrated for offshore plate anchors, the proposed framework is readily transferable to uncertainty quantification problems across a broad range of geotechnical engineering applications.

Keywords Bayesian inference · Stochastic surrogate model · Plate anchor · Inverse problems · Monte Carlo · Polynomial Chaos Expansion · Offshore structures · Probabilistic modelling

List of symbols

V, H, M	Vertical load, horizontal load and moment on the plate anchor (kN/m, kN/m, kN·m/m)
V_0, H_0, M_0	Uniaxial (pure-mode) ultimate capacities of the plate anchor in *V*-, *H*- and *M*-directions
$V_{load}, H_{load}, M_{load}$	Applied vertical, horizontal and moment load components used in the finite-element loading
V_{cap}, H_{cap}	The output variables of surrogate models predict the ultimate bearing capacity of plate anchors in both vertical and horizontal directions.
$d = V, H, M$	Observed load vector used as data in the Bayesian likelihood
N_v, N_h, N_m	Dimensionless bearing-capacity factors associated with V_0, H_0 and M_0
$\{m, n, p, q\}$	The exponential parameter of the *V-H-M* yield surface (failure envelope) shape.
θ	Vector of yield-surface parameters, $\theta = \{N_v, N_h, N_m, m, n, p, q$
S_u	Undrained shear strength of the clay (kPa)
E_u	Undrained Young's modulus, taken as Eu = 500 *su* (kPa)
B	Width of the plate anchor (m)
L	Length of the plate anchor (plane strain, $L = B$) (m)
t	Thickness of the plate anchor (m)
D	Embedment depth of the plate anchor (m)
x_{mesh}	Dimensionless mesh-refinement factor controlling element size around the anchor
d_m	Characteristic element size in the refined zone, $d_m = 4t/x_{mesh}$
$d_{m,min}$	Minimum element size, $d_{m,min} = t/x_{mesh}$
x_M	Moment Factor, $x_M = M/M_0$
x_α	Displacement (load inclination) factor, $x_\alpha = \alpha/(\pi/2)$
α	Inclination angle of the resultant in-plane load (rad)
X	Vector of standardised random input variables to the PCE surrogate
$p(\theta)$	Prior distribution of θ
$p(d\|\theta)$	Likelihood of observing d given θ
$p(\theta\|d)$	Posterior distribution of θ given d
σ	Standard deviation of the Gaussian likelihood noise (kN/m)
$\mathcal{F}_\mathcal{V}, \mathcal{F}_\mathcal{H}$	The PCE models for the vertical and horizontal capacities
R	Gelman–Rubin convergence diagnostic for MCMC chains
Y	Stochastic response variable predicted by the PCE surrogate
Y	Vector of observed training-sample responses
$\Psi_k(X)$	*k*-Th multivariate orthogonal polynomial basis function
c_k	*k*-Th PCE expansion coefficient
P	Highest polynomial order retained in the PCE
$\mathrm{P}+1$	Number of terms in the truncated PCE basis
A	Design (information) matrix, $A \in R^{N\times(P+1)}$
$S_{1,i}$	First-order Sobol sensitivity index for input variable i
$S_{T,i}$	Total-effect Sobol' sensitivity index for input variable i
R^2	Coefficient of determination used to assess PCE accuracy
$\mathrm{y_i}, \hat{y}_i$	*i*-Th observed and PCE-predicted response value, respectively
κ	Normalised undrained shear strength, $\kappa = s_u/s_{u,ref}$ $s_{u,ref} = 6kPa$ (dimensionless)
$\kappa(\mathrm{A})$	Condition number of the PCE design matrix
kPa	Kilopascal

m	Metre
kN	Kilonewton

1 Introduction and Background

Uncertainty quantification (UQ) has become increasingly important in geotechnical engineering, particularly in offshore, due to the inherent variability and measurement/estimation uncertainty in soil properties and behaviour, and the uncertainty associated with empirical, analytical and numerical solutions developed for engineering design of offshore systems. The Bayesian approach has become a widely adopted framework for uncertainty quantification and solving inverse problems across various disciplines, offering a systematic way to integrate prior knowledge with observations/data. In engineering, Bayesian methods have gained significant traction in mechanics (Rappel et al. 2020; Weisz-Patrault et al. 2021), structures (Vilares and Kording 2011; Ballesteros et al. 2014), and geotechnics (Juang et al. 2013; Ching and Phoon 2019; Zhou et al. 2021; Yousefpour et al. 2021).

Bayesian methods have been widely used for uncertainty quantification and probabilistic inference of geotechnical properties and model parameters. Phoon and Kulhawy (1999) and Juang et al. (2013) provided a comprehensive review of Bayesian inference for geotechnical applications. These studies highlight the growing interest in Bayesian methods for solving inverse problems and quantifying uncertainties in offshore and geotechnical engineering. Bayesian inference has been used for site characterization (Wang et al. 2016; Ching and Phoon 2019) to estimate soil design parameters, analyse slope stability (Zhang et al. 2010), retaining walls, braced excavations (Qi and Zhou 2017), and for model calibration (Zhang et al. 2012), reverse engineering and inverse problems (Medina-Cetina et al. 2020; Yousefpour 2013).

Development of both efficient forward and backward models (models that map observations directly to model parameters) are essential components in the Bayesian uncertainty quantification. In many complex engineering problems, however, propagating the quantified parameter uncertainties through forward models to predict system response presents a major computational challenge. This is because in many engineering processes, especially those described by partial differential equations, analytical solutions are not available. In such cases, numerical methods are applied to approximate the forward model and give rise to the numerical approximation errors. Monte-Carlo (MC) method is often used to propagate the uncertainty from the model parameters to model predictions. However, in case of complex forward models running the MC uncertainty propagation can be computationally intensive, as it requires the forward model to be evaluated for each sample. This computational bottleneck often limits the application of rigorous UQ in routine geotechnical design.

An alternative approach to avoid running the forward model for each sample is to represent the stochastic process using series analogues to Fourier-type such as Polynomial Chaos (PC) and Karhunen–Loeve (KL) expansion methods (Marzouk et al. 2007). These polynomial-based models can serve as surrogates for the forward models for much more efficient uncertainty quantification. A key advantage of these stochastic polynomial models over other surrogate/meta-modelling methods is that they provide closed-form analytical expressions relating the input random variables to the output of interest, meaning that practitioners can evaluate the surrogate by simple polynomial arithmetic without requiring specialised simulation software. This transparency is particularly appealing in geotechnical engineering practice.

The KL method, first derived by Karhunen (1946) and Loeve (1963), expands the process function by the spectral decomposition of the corresponding covariance function of the process. Wiener (1938) first introduced the theory of the Homogeneous Chaos, and Ghanem and Spanos (1991) implemented the Polynomial Chaos method into the finite element context. This method suggests the spectral expansion of random variables and stochastic processes using a set of orthogonal polynomials and has been successfully applied for uncertainty assessment in various fields including structural mechanics (Ghanem 1999), flow and transport in porous media (Dostert et al. 2008; Ghanem and Dham 1998; Ghanem 1999; Yang et al. 2004), fluid dynamics (Mathelin et al. 2005; Najm 2009), and diffusion problems (Xiu and Karniadakis 2002; Tuminaro et al. 2011).

Surrogate modelling techniques have also been applied in offshore geotechnics for uncertainty quantification and reliability analysis (Charlton and Rouainia 2019; Shen et al. 2020; Suryasentana et al.

2024). Also, surrogate-based reliability analysis has gained increasing attention in geotechnical engineering. Recent studies have demonstrated the effectiveness of machine learning and polynomial-based surrogates for efficient reliability estimation, including optimization-based calibration of load and resistance factors using adaptive metamodels (Doan et al. 2022). These developments underscore the growing importance of computationally efficient surrogate methods for uncertainty quantification in geotechnical and offshore engineering practice.

Predicting offshore foundation capacity is inherently challenging due to uncertainties from complex loading and variable soil properties. These challenges often arise from numerical modelling techniques and dynamic offshore environments. For the numerical modelling, the accuracy of capacity predictions is influenced by mesh discretisation and constitutive model assumptions. Additionally, the inherent variability of soil properties adds another layer of uncertainty to the analysis. To assess the uncertainties efficiently, stochastic surrogate models are increasingly employed to replace computationally demanding numerical simulations. For instance, sparse polynomial chaos expansions (SPCE) and random field modelling have been applied to investigate the probabilistic failure envelopes of strip foundations considering non-stationary soil characteristics (Shen et al. 2023) and to analyse skirted foundations under combined loading in similar non-stationary soil conditions (Chen et al. 2023). Similarly, Mentani et al. (2023) incorporated PCE models to predict the pull-out capacity of steel piles driven in offshore sand, demonstrating the capability of PCE metamodels for replacing laborious and computationally expensive finite element simulations.

More recent studies further reflect this trend across geotechnical applications: Tran et al. (2025) developed machine-learning surrogates of V–H–M failure envelopes for strip anchors based on finite element limit analysis, Vichai et al. (2025) applied soft-computing models to predict three-dimensional failure envelopes of skirted foundations in heterogeneous clays, and Menaka et al. (2026) employed multivariate adaptive regression splines for the reliability analysis of deep excavations. Within stochastic polynomial approaches, Li et al. (2026) proposed an active learning-based sparse PCE method for efficient reliability analysis of geotechnical structures.

This paper presents a framework for uncertainty quantification of plate anchor capacity integrating Bayesian inference with PCE surrogate modelling. Bayesian inference is employed to calibrate the physical model parameters of an analytical yield surface, and PCE is subsequently used both as a validation surrogate for the calibrated analytical model (Workflow A) and as a direct replacement for computationally expensive finite element simulations (Workflow B). This two-workflow architecture provides a systematic strategy for validating the PCE methodology in a controlled setting before deploying it in practice. The application of advanced surrogate stochastic modelling techniques for comprehensive uncertainty quantification of plate anchors capacity has been limited (Charlton and Rouainia 2019; Mentani et al. 2025). This is the first study that addresses both parametric uncertainties and numerical approximation error using PCE method for plate anchors under combined $V-H-M$ loading, also comparing PCE with a Bayesian probabilistic analytical model.

To clearly demonstrate the framework's capabilities, this study utilizes a deliberately simplified case study based on an elasto- perfectly plastic soil model that neglects time-dependent effects. Although the present case study adopts a simplified elasto-perfectly plastic soil model that does not explicitly incorporate cyclic loading, installation effects, or seabed spatial variability, the problem formulation, encompassing the anchor geometry, deep embedment ratio, $V-H-M$ combined loading framework, and undrained shear strength range representative of deepwater soft clays, is directly relevant to offshore plate anchor design. The simplifications are deliberate, intended to provide a transparent demonstration of the UQ framework without the confounding influence of more complex soil behaviours. This framework is applicable for broader range of geosystems, particularly in foundation design, and aims to:

- Quantify uncertainties in model parameters of analytical capacity equation, using Bayesian inference conditioned on high-fidelity finite element data.
- Develop and compare a PCE surrogate with the probabilistic analytical model
- Construct a direct PCE surrogate of the computationally expensive FE model to facilitate UQ for

complex soil and loading condition, where an analytical model is not applicable/available.
- Systematically assess the impact of different sources of uncertainty, including loading, soil strength and numerical approximation error (mesh discretisation) on the anchor capacity.

It is worth noting that the recent studies have explored the coupling of Bayesian methods with PCE to infer PCE coefficients (Bhattacharyya 2020) and for Bayesian adaptive sparse-basis selection (Rumsey et al. 2026) for PCE construction. In this study, Bayesian inference is used to calibrate the physical model parameters of the analytical yield surface to provide basis of comparison and validation for the PCE surrogate for uncertainty propagation. A fixed full-tensor second-order basis is adopted for transparency and reproducibility, which is sufficient given the input dimensionality considered.

The behaviour of plate anchors under combined vertical V, horizontal H, and moment M loading has been studied extensively using failure envelope formulations. Taiebat and Carter (2000) conducted numerical studies of combined-loading failure criteria for foundations on cohesive soil, establishing fundamental $V-H-M$ interaction principles for embedded geotechnical elements. Randolph and Puzrin (2003) developed upper bound solutions for embedded foundations under general loading in non-uniform clay, providing $V-H-M$ interaction frameworks directly applicable to deeply embedded plate anchor problems. Yang et al. (2010) directly characterised the undrained capacity of plate anchors under general combined loading through finite element analyses, demonstrating the three-dimensional nature of the failure surface in $V-H-M$ load space. Recent numerical studies continue to advance plate anchor capacity assessment, including limit analysis of the pullout resistance of plate anchors in anisotropic and non-homogeneous clays (Mushtaq and Sahoo 2026) and quantification of the coupled effects of factors influencing plate anchor capacity in clay (Peng and Yin 2026).

The phenomenological yield surface equation proposed by Elkhatib (2005) was adopted as the analytical backbone of the present study for its flexible parametric representation of the three-dimensional failure surface, and its direct calibration to finite element analyses for deeply embedded plate anchors in clay. The formulation also has known limitations: it was calibrated for a specific anchor geometry and embedment depth range, assumes a smooth soil-anchor interface, and does not explicitly account for excess pore-pressure generation or rate-dependent effects. Notwithstanding these limitations, the Elkhatib (2005) model is considered fit for purpose for the present study, which focuses on development of stochastic surrogate modeling framework.

Finally, this study does not consider spatial variability as a source of uncertainty. It focuses on the epistemic uncertainties of modeling plate anchor capacity under multi-axial loading. It considers undrained soil strength, s_u(averaged), spatially uniform at the anchor embedment depth rather with on spatial fluctuations within the soil domain; this treatment is consistent with the Vanmarcke (1977) framework for cases in which the failure mechanism volume is small relative to the autocorrelation scale, such that the spatial average is statistically equivalent to a single representative value. Soil spatial variability in geotechnical systems is rigorously characterised by random field methods, which represent soil properties such s_u as spatially correlated random processes defined by their autocorrelation length scale and the Vanmarcke variance-reduction factor (Vanmarcke 1977; Phoon and Kulhawy 1999; Griffiths and Fenton 2004).

Recent studies have applied random field modelling to investigate the effects of spatial variability on anchor capacity; for instance, Hwang and Lee (2025) demonstrated through adaptive finite element limit analysis with random fields that ignoring the spatial variability of undrained shear strength leads to systematic overprediction of inclined strip anchor resistance, with the effect being more pronounced for deeply embedded anchors. He et al. (2025) performed probabilistic design analyses of plate anchors in spatially variable clay using the random finite element method, while Tom et al. (2025) quantified the reliability of dynamically embedded anchors in soft clay through Monte Carlo simulation.

2 Methodology

The methodology presented in this section is formulated as a general uncertainty quantification framework applicable to a range of geotechnical problems. The framework consists of three modular components: (i) Bayesian inference for calibrating uncertain model parameters against observed or simulated data, (ii) PCE surrogate construction for efficient uncertainty propagation, and (iii) systematic assessment of multiple uncertainty sources. These components require only a forward model, whether analytical or numerical, that maps input parameters to a response of interest, and a set of observations for calibration and training. The forward model can be readily substituted to address other geotechnical applications, such as shallow foundation design, pile capacity prediction, or slope stability analysis. In the following subsections, the framework is demonstrated through a plate anchor case study, which serves as a representative example of offshore foundation problems involving combined loading and multiple uncertainty sources.

2.1 The Finite Element Model

A two-dimensional plane strain Finite Element (FE) model of a deeply embedded plate anchor is developed using the commercial software Abaqus to investigate the anchor capacity under general $V-H-M$ loading.

A unitary size (i.e., $B = 1m$) is adopted as a normalisation convention, consistent with Elkhatib and Randolph (2005). Because the analysis is conducted under plane strain conditions, all loads are computed per unit out-of-plane length (kN/m for forces, kN m/m for moments); the out-of-plane reference length L is likewise set to 1 m so that the per-unit-length capacities are numerically compatible with the general three-dimensional definitions. With $L = B = 1m$, the capacity factors reduce to dimensionless ratios $N_v = V_0/s_u$, $N_h = H_0/s_u$, and $N_m = M_0/s_u$, directly comparable to published plane strain bearing capacity factors (e.g., Taiebat and Carter 2000; Randolph and Puzrin 2003). This approach does not restrict the generality of the findings, as the capacity factors are dimensionless and applicable to any geometrically similar anchor. The thickness ratio B/t is set to 20 as Elkhatib and Randolph (2005). The anchor is embedded to a depth $D = 6B$, as shown in Fig. 1a to ensure deep failure mechanisms to loading, while the external size of the model is set to $12B$, which prevents any boundary effect. The soil domain is restrained to horizontal displacements on the lateral sides, while vertical boundary conditions are applied at the base (Fig. 1a).

The FE mesh is discretised with 4-node quadrilateral elements with a refined mesh applied within a $3B \times 2B$ region around the plate anchor (Fig. 1 b), where the kinematic failure mechanisms are expected to develop. The smallest elements adjacent to the anchor have a side length $d_{m,min} = t/x_{mesh,}$ where x_{mesh} is a mesh factor which was varied to analyse the impact of numerical approximation error (mesh

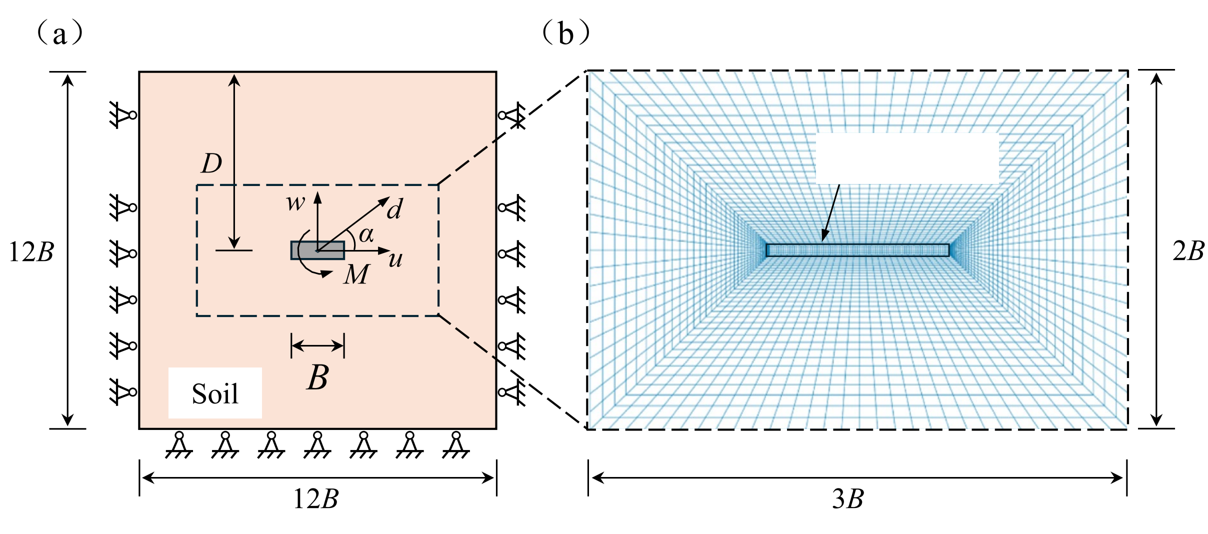

Fig. 1 The 2D finite element model setup for the plate anchor analysis: **a** geometry, boundary conditions, and loading configuration; **b** refined mesh in the $3B \times 2B$ region around the anchor

discretisation) on capacity predictions, as described in Sect. 2.4.1. The element size gradually increases to $d_m = 4t/x_{mesh}$ at the outer edge of the refined region.

The soil is modelled with a linear elastic perfectly plastic material, while the anchor is modelled as a rigid body with loads applied at its centroid. The soil elastic response is defined by a Young's modulus $E_u = 500 s_u$ kPa and a Poisson's ratio set to 0.49, the latter chosen for numerical stability while approximating the incompressible behaviour of saturated clay under undrained condition. The plastic response is governed by a Tresca criterion, with the undrained shear strength s_u defining the limit of the yield surface. The use of an elastic-perfectly plastic model with a Tresca failure criterion is widely accepted simplification for total stress analysis in undrained conditions, providing a robust baseline for assessing bearing capacity. A fully bonded contact law is assumed at the soil-anchor interface as undrained conditions are simulated (Wang et al. 2010).

Displacement-controlled FE analysis (FEA) is carried out to determine the uniaxial capacities of the plate anchor. The uniaxial vertical (V_0), horizontal (H_0), and moment (M_0) capacities are defined here as the ultimate (uniaxial) vertical, horizontal and moment capacities of the anchor, obtained from three independent pure-component FE analyses with vertical and horizontal translation (w and u), and rotation applied at the anchor's centroid. The ultimate capacities (V_0, H_0, M_0) are defined as the limiting, asymptotic load values obtained when the load–displacement curves reach a clear plateau.

For general loading conditions, a two-stage probe is implemented to map out the yield locus. The anchor is initially prescribed a constant moment M, defined as a ratio to the uniaxial capacity M_0 by the moment factor x_M (i.e., $x_M = M/M_0$). Holding the moment constant, a displacement-controlled probe is applied at the centroid with a constant horizontal to vertical displacement path defined by the vector d and the angle α, shown in Fig. 1a. The latter is specified by the displacement factor (load inclination factor) x_α which governs its magnitude (i.e., $\alpha = x_\alpha \pi/2$). The coefficients x_M and x_α defining the anchor load paths are varied between 0 to 1 on a deterministic 5×5 design-of-experiment (DoE) grid resulting in 25 combinations per s_u value. These are controlled sweep variables that map out the failure envelope, and the uniform sweep characterises the complete envelope rather than a calibrated stochastic load model and the FEA run until plastic failure is reached. The resulting V and H load points, together with the input M, are used to describe the full yield locus of the anchor.

2.2 The Analytical Model and Bayesian Inference

A semi-empirical equation (referred to as analytical thereafter) for plate anchor capacity in general V-H-M load space was proposed by Elkhatib (2005):

$$\left(\frac{V}{V_0}\right)^q + \left[\left(\frac{|M|}{M_0}\right)^m + \left(\frac{|H|}{H_0}\right)^n\right]^{\frac{1}{p}} - 1 = 0 \tag{1}$$

where $\{m, n, p, q\}$ are model parameters defining the shape of the three-dimensional failure surface.

This equation is generalized by defining non-dimensional capacity factors, N_v, N_h, and N_m derived from normalizing the uniaxial vertical, horizontal, and moment capacities by the soil shear strength and the plate anchor geometry:

$$N_v = V_0/\left(s_u LB\right) \tag{2}$$

$$N_h = H_0/\left(s_u LB\right) \tag{3}$$

$$N_m = M_0/\left(s_u LB^2\right) \tag{4}$$

Under the plane strain convention adopted in Sect. 2.1, the anchor is analysed per unit out-of-plane length, so L and B are both set to 1 m. In Eqs. (2)–(4), the groupings s_uLB and s_uLB^2 act as a reference force and reference moment that non-dimensionalise the capacities. Substituting $L = B = 1m$ reduce the yield surface to:

$$\left(\frac{V}{s_u N_v}\right)^q + \left[\left(\frac{M}{s_u N_m}\right)^m + \left(\frac{H}{s_u N_h}\right)^n\right]^{\frac{1}{p}} - 1 = 0 \tag{5}$$

It is important to note that this equation represents a phenomenological failure surface, designed to mathematically capture the complex three-dimensional $V - H - M$ load space of the anchor (Elkhatib 2005). The parameters $\{N_v, N_h, N_m, m, n, p, q\}$ are calibration coefficients governing the geometry of the normalized yield surface and are inferred from observations. Their inferred values are therefore conditioned on the calibration dataset used. Therefore, these model parameters are not deterministic and are subjected to epistemic uncertainty arising from the calibration process. This simplified equation forms the likelihood function for the subsequent Bayesian inference in this study, capturing the relationship between the anchor capacities, soil strength, and model parameters under plane strain conditions.

Considering $\theta = \{N_v, N_h, N_m, m, n, p, q\}$, the vector of model (uncertain) parameters and $d = \{V, H, M\}$ the vector of new observations of the process (obtained from high-fidelity Finite Element simulations), $p(\theta)$ represents the prior distribution and $p(d|\theta)$ represents the likelihood. The core idea of Bayesian inference here is to update our knowledge about the uncertain analytical model parameters θ in light of the observed data d from the FE model. We start with a prior belief about the parameters $p(\theta)$, and the inference process yields a posterior distribution $p(d|\theta)$ that represents our updated, more informed belief. According to Bayes' theorem, the posterior probability density of model parameters given the observed data, can be written as:

$$p(\theta|d) = \frac{p(\theta)p(d|\theta)}{\int p(\theta)p(d|\theta)d\theta} \tag{6}$$

The prior distributions of the uncertain parameters in Eq. (6) are modelled as uniform distributions with bounds based on the values reported in Elkhatib (2005) (see Table 2). Uniform distributions are adopted as the maximum-entropy (least-informative) prior choice when only the physically plausible parameter range is known, ensuring that no unintended bias is introduced into the inference process. The prior bounds are taken directly from the parameter ranges reported by Elkhatib (2005), representing physically meaningful limits of the yield surface shape parameters for deeply embedded plate anchors in soft clay.

The likelihood function is defined assuming a normal distribution for the model error:

$$p(d|\theta) = \frac{1}{\sqrt{2\pi\sigma^2}} \exp\left(-\frac{1}{2\sigma^2}\left[\left(\frac{V}{s_u N_v}\right)^q + \left(\left(\frac{M}{s_u N_m}\right)^m + \left(\frac{H}{s_u N_h}\right)^n\right)^{\frac{1}{p}} - 1\right]^2\right) \tag{7}$$

This likelihood function, $p(d|\theta)$, quantifies how probable it is to observe the FEA data (treated here as "*ground truth*") d, given a specific set of the analytical model's parameters θ. The function assumes that the analytical model (Eq. (5)) is not a perfect representation of the FEA results, and the discrepancy (or model error) follows a zero-mean normal distribution with standard deviation (SD). The model error standard deviation σ is treated as an additional uncertain parameter with a uniform prior $\sigma \sim U(0, 10)kN/m$ and is inferred jointly with the yield-surface parameters θ via MCMC. The goal is to find the parameter set θ that makes the observed data most plausible (i.e., maximizes the likelihood), while also being consistent with our prior knowledge about model parameters.

Markov Chain Monte Carlo (MCMC) sampling, specifically the Metropolis–Hastings algorithm (Chib and Greenberg 1995) implemented in the PyMC library (Patil et al. 2010), is used to generate samples from the posterior distributions. Convergence was assessed by running four independent Metropolis–Hastings chains for each inference, each with 50,000 post-tuning draws and initial values drawn uniformly at random from the prior bounds. The Gelman–Rubin statistic $\hat{R}$, the bulk effective sample size (ESS), and the Metropolis acceptance rate were computed for all seven parameters; the resulting diagnostics are reported in Sect. 3.1.1.

2.3 Polynomial Chaos Expansion

In this study, PCE is employed to construct surrogate models for the plate anchor capacity under combined loading scenarios. Conceptually, PCE is a powerful surrogate modelling technique that approximates a complex, potentially computationally expensive model with a much simpler and faster polynomial function. This surrogate is constructed in a mathematically rigorous way to capture how the uncertainties from the model's input variables propagate to its output. The PCE methodology adopted here follows the generalized framework described by Xiu and Karniadakis (2002) and Ghanem and Spanos (1991), where a stochastic output Y (V or H, i.e., vertical or horizontal anchor capacity) is expressed as a spectral expansion in terms of orthogonal polynomial basis functions of the input random variables X:

$$Y = \sum_{k=0}^{P} c_k \Psi_k(X) \tag{8}$$

where $\boldsymbol{X}$ denotes the input variables, $\Psi_k(X)$ are multivariate orthogonal polynomial basis functions indexed by k, and c_k are the deterministic PCE coefficients. The total number of terms in the PCE expansion (Eq. (8)), $P+1$ depends on the polynomial degree p and the input dimension n, as:

$$P + 1 = \frac{(n+p)!}{n!p!} \tag{9}$$

The input variables include mechanical loads (M, H or V), s_u, and the model parameters. These variables vary in different experiment groups in this paper. The polynomial basis Ψ_k is selected based on the probability distribution of each input variable. The Hermite polynomials are used for Gaussian variables (e.g., parameters in θ), and Legendre polynomials are selected for uniformly distributed variables (e.g., x_M).

For the present application with $n \leq 9$ input variables, a full-tensor second-order polynomial basis is employed, retaining all possible interaction and quadratic terms without truncation or sparsification. This approach is conceptually distinct from adaptive sparse regression methods such as least-angle regression (Blatman and Sudret 2011), LASSO (Tibshirani 1996), and Bayesian compressive sensing (Sargsyan et al. 2014), which select a sparse subset of basis functions and are better suited to high-dimensional problems ($n \geq 20$). The full-tensor ordinary least squares (OLS) approach adopted here is transparent, deterministic, and numerically well-conditioned for the input dimensionalities considered in this study. A systematic comparison of polynomial orders 1, 2, and 3 confirms that the second-order expansion provides the optimal balance between accuracy and model complexity, with negligible improvement from third-order terms. The design matrix condition numbers $\kappa(A)$ are reported for all PCE models to verify numerical stability; the full convergence table is included in the Supplemental Materials.

The PC expansion coefficients c_k are deterministic and can be found through various methods forming two broad categories of intrusive and non-intrusive methods (Reagan et al. 2003; Eldred and Burkardt 2009; Ghanem et al. 2000). In this paper, the coefficients $\boldsymbol{c} = \{c_k\}$ are estimated using the *Chaospy* library (Feinberg and Langtangen 2015). This library simplifies the complex process of selecting the appropriate orthogonal polynomials based on the distribution of the input variables and constructing the design matrix $A \in R^{N\times(P+1)}$, in which each row corresponds to a specific training data point and each column represents a polynomial basis function evaluated at that point, needed to solve for the coefficients via least squares regression. The least squares solution (Eldred and Burkardt 2009) is obtained via:

$$c = \left(A^T A\right)^{-1} A^T Y \tag{10}$$

where Y is the vector of observations (anchor capacities from analytical/FE simulations). The Cholesky decomposition ensures numerical stability during polynomial generation. The accuracy of the PCE models is assessed by comparing their predictions to the observations. Validation metrics such as mean squared error (MSE) and coefficient of determination (R^2) are used to quantify the goodness-of-fit. The computational cost of the PCE models is also evaluated to demonstrate their utility in performing uncertainty quantification and sensitivity analysis.

The tensor-product polynomial basis in Eq. (8) presumes that the input random variables X are mutually independent. For problems in which the inputs exhibit non-negligible statistical dependence, an isoprobabilistic transformation to independent standard variables (Rosenblatt 1952) or a generalised PCE formulation for dependent inputs (Soize and Ghanem 2004; Jakeman et al. 2019) should be applied prior to basis construction. The applicability of the independence assumption to the inputs of Workflows A and B in the present study is discussed in Sects. 3.1.2 and 3.2, respectively.

A key strength of PCE over black-box surrogates is that the orthogonality of the polynomial basis enables a direct analytical decomposition of the output variance into contributions from individual inputs and their interactions (Sudret 2008). The first-order Sobol sensitivity index for input variables is:

$$S_{1,i} = \frac{\sum_{k\in\mathcal{A}_i} c_k^2}{\sum_{k=1}^{P} c_k^2} \tag{11}$$

where $\mathcal{A}_i$ is the set of indices of basis terms that depend only on variable i (i.e., terms in which the multi-index has a non-zero entry for variable i and zero entries for all other variables). The total-effect index $S_{T,i}$ is obtained by summing over all basis terms that contain variable i (including interaction terms):

$$S_{T,i} = \frac{\sum_{k\in\mathcal{A}_i^{\mathcal{T}}} c_k^2}{\sum_{k=1}^{P} c_k^2} \tag{12}$$

where $\mathcal{A}_i^{\mathcal{T}}$ is the set of indices of all basis terms with a non-zero entry for variable i. The Sobol indices for PCE Models A and B are reported in Sects. 3.1.2 and 3.2, respectively.

2.4 Uncertainty Quantification Framework

This framework employs two distinct experimental workflows, designated as Workflow A and Workflow B, to systematically quantify the uncertainties in plate anchor capacity. As illustrated in Fig. 2, these workflows are designed to assess uncertainties from different sources and to evaluate the performance of the PCE surrogate models. Workflow A serves as a methodological validation step rather than an engineering necessity: the analytical equation itself is computationally inexpensive, and the purpose of building a PCE surrogate for it is to verify the accuracy and convergence of the PCE method in a controlled setting before deploying it on the computationally demanding FE model in Workflow B. Workflow A also allows for evaluation of yield surface model parameter uncertainties and effect of soil strength uncertainty and numerical approximation error (mesh size) on the inferred model parameters and the estimated anchor capacities. Workflow B, in contrast, demonstrates the primary practical application of the framework by using PCE to directly replace computationally expensive FE simulation, focusing on evaluating the effects of undrained shear strength and loading inclination uncertainties on the estimated anchor capacities. The specific data samples used, and the detailed execution of these workflows are described in the subsequent subsections.

2.4.1 Sampled Data/Observations

The impact of the uncertainty of the model parameters θ and soil strength s_u on the plate anchor capacity is assessed through observations/data from a series of FEA simulations, providing anchor capacities V and H at failure for combinations of x_M and x_α, for each s_u value. To investigate the effect of uncertainty in undrained shear strength of soil, 100 Monte Carlo random samples were first drawn from $\kappa \sim N(1.5{,}0.3)kPa$, where $\kappa = s_u/D$ is the normalised strength ratio (D = 6B, equivalently $s_u \sim N(9{,}1.8)kPa$, $COV = 0.2$). From these 100 samples, 19 values spanning the full distribution range $s_u = (5.88 - 11.76)kPa$, were selected for finite element simulation. The choice of

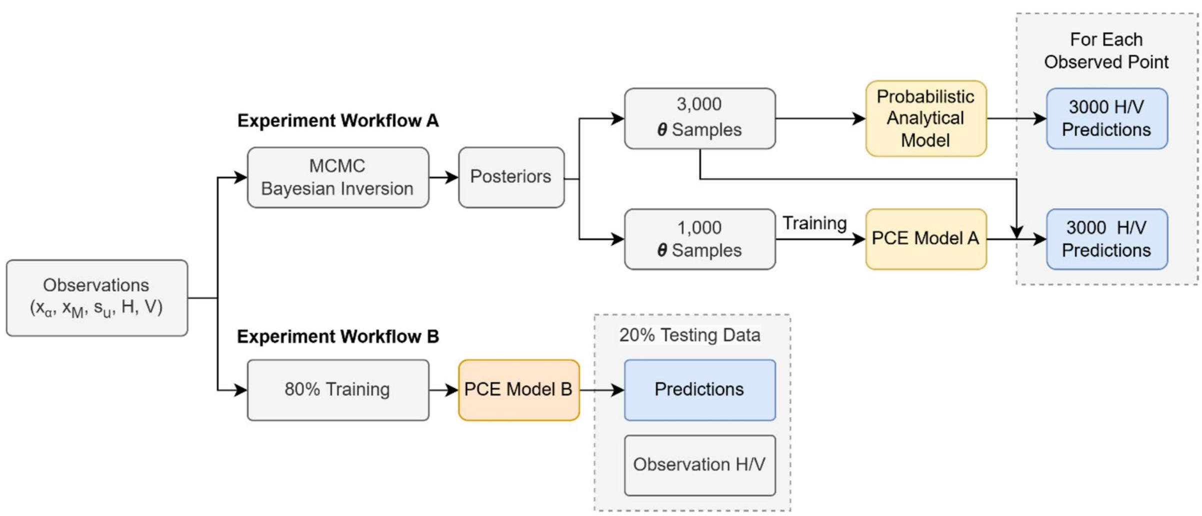

Fig. 2 Schematic overview of the uncertainty quantification workflows

19 was governed by the computational budget: each s_u value requires 25 loading combinations (5 x_M levels×5 x_α levels), yielding $19 \times 25 = 475$ FE simulations; using all 100 samples would require approximately 2500 simulations, which was computationally prohibitive. These nineteen distinct s_u values were sampled from a normal distribution $N(9kPa, 1.8kPa)$, representing the uncertainty in the spatially averaged s_u at the anchor embedment depth. Each s_u value represents a spatially uniform soil condition, and soil spatial variability is not considered in the present study. The s_u was considered to be linearly increasing with depth with a rate of $1-2kPa/m$. This sampling resulted in values primarily ranging from approximately 6 to 12 kPa, representative of the strength at the anchor's embedment depth ($D = 6B = 6m$).

For each s_u value, simulations were performed using all combinations of proportional moment x_M = [0,0.2,0.4,0.6,0.8] and displacement factor $x_\alpha = [0, 0.25, 0.5, 0.75, 1]$. These ranges were selected to encompass the full spectrum of loading conditions. The two factors are not treated as random variables but are combined through a deterministic full-factorial design: the five prescribed levels of x_M are crossed with the five prescribed levels of x_α, yielding $5 \times 5 = 25$ loading combinations per s_u value. Each $\left(x_M, x_\alpha\right)$ pair defines a distinct deterministic loading path, providing a uniform parametric sweep of the $V-H-M$ load space for calibrating the yield-surface model and training the PCE surrogate. Figure 3 illustrates the anchor capacity data generated from FEA, which serves as the observations for the subsequent uncertainty analysis. Figure 3a shows the failure envelopes for a range of s_u values (6–12 kPa). As expected, higher s_u values lead to higher capacities and an expanded failure surface.

To investigate the impact of numerical approximation error due to mesh discretisation, simulations

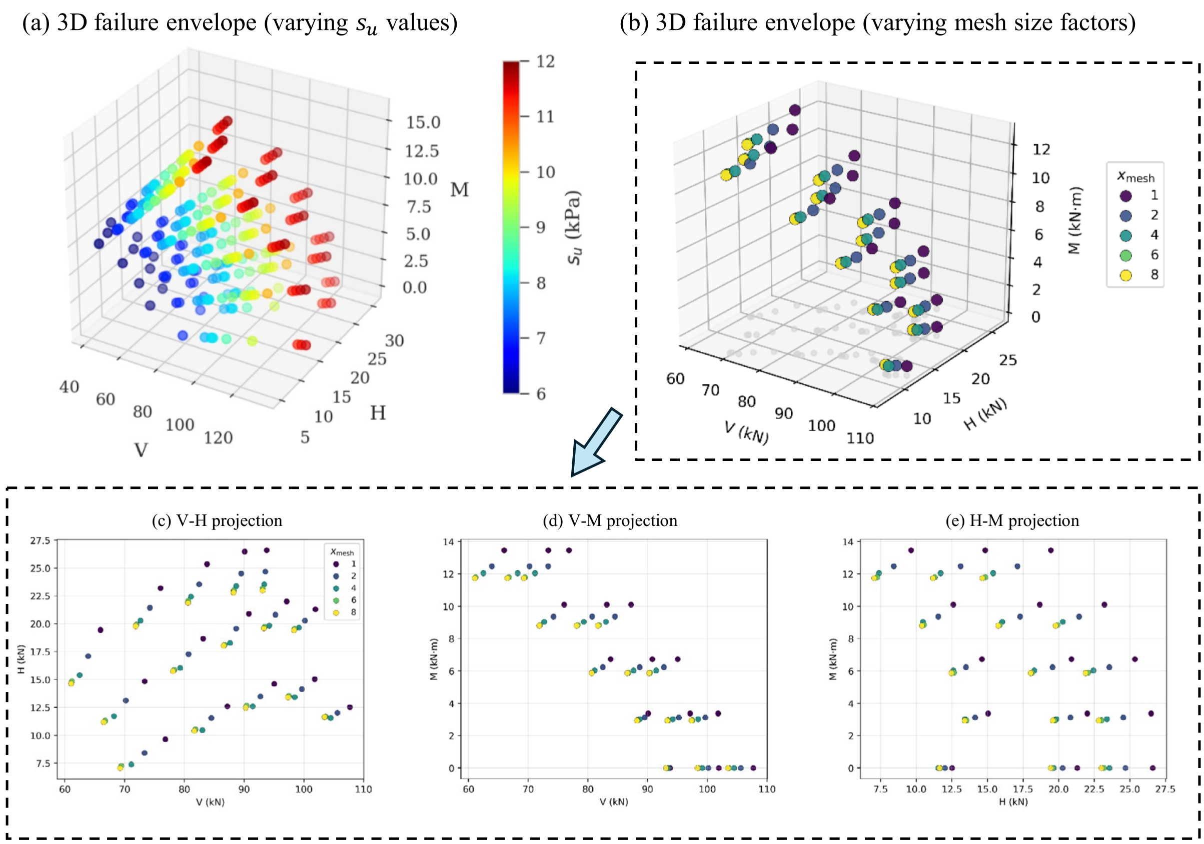

Fig. 3 Plate anchor capacities obtained from FEA, illustrating the influence of **a** varying s_u values with a fixed mesh size ($x_{mesh} = 4$), and **b** varying mesh size factors with a fixed s_u (9 kPa). This data forms the "observations" for the uncertainty and numerical approximation error analyses

were also run with five different mesh size factors ($x_{mesh} = [1, 2, 4, 6, 8]$), while keeping s_u fixed at 9 kPa, as shown in Fig. 3b. The mesh convergence study showed that the predicted capacity obtained with $x_{mesh} = 4$ differed by less than 1% from the finest mesh, while requiring substantially lower computational effort. Therefore, it was selected as the baseline discretisation for the subsequent analyses. Mesh discretisation is one of several sources of numerical approximation error in finite element analysis, together with temporal discretisation, solver convergence, numerical integration, and round-off errors. However, discretisation error is widely recognised as the dominant source of numerical uncertainty in finite element simulations (Oberkampf and Roy 2010). In this study, mesh resolution is the only numerical hyperparameter varied and therefore governs the numerical approximation uncertainty in the plate anchor finite element simulations.

2.4.2 Uncertainty Quantification Workflows

Two distinct experimental workflows, Workflow A and Workflow B, are employed as shown in Fig. 2. These workflows utilise datasets ('Observation Samples' in Table 1) generated from the FEA simulations described in Sect. 2.1. The FEA simulations provide the 'observations' (anchor capacities V, H, M at failure) used in our uncertainty analysis. These observations were generated by running the FEA model for various combinations of input parameters, including:

- Loading path factors: moment factor (x_M) and displacement factor (x_α).
- Undrained shear strength (s_u)
- Mesh factor (x_{mesh})

Table 1 summarizes the specific subsets of these FEA observations used for each distinct numerical experiment (A1, A2, A3, B1). It details the specific s_u values (fixed or varying) and x_{mesh} values associated with the observation samples used in each workflow, along with the objective of that particular numerical experiment.

Experiment Workflow A (top path, used in Exp. A1-A3) aims to validate the PCE methodology. It uses FEA 'Observations' to calibrate the analytical model's parameters (θ) via MCMC Bayesian Inversion, yielding posterior distributions. Samples from these posteriors are then used in parallel to: (i) run a full probabilistic analysis with the analytical model, and (ii) train and test a surrogate, PCE Model A. The goal is to show that PCE Model A's predictions match the analytical models. Experiment Workflow B (bottom path, used in Exp. B1) demonstrates the practical use of PCE for replacing expensive simulations. It

Table 1 Summary of Experiments–See Details on observation sample generation in Sect. 2.4.1 (Exp. is Experiments, and W.F. is Workflow)

Exp	W.F	Observation samples	s_u(kPa)	Mesh Size factor x_{mesh}	Objective
A1	A	25	9	4	Model parameters uncertainty quantification (baseline): quantify the uncertainty of plate anchor capacity due to uncertainty in the analytical model parameters θ, using both analytical and PCE solutions, under baseline s_u and mesh size
A2	A	430	Varying values from $N(9, 1.8) kPa$	4	Soil strength uncertainty: validate the structural independence between s_u and yield-surface shape parameters θ under realistic uncertain s_u conditions and quantify the combined effect of parameter uncertainty and soil strength uncertainty on anchor capacity predictions using both the probabilistic analytical model and the PCE surrogate
A3	A	75	9	Varying values from [1, 2, 4, 6, 8]	Numerical approximation error: quantify the effect of numerical approximation error (mesh discretisation) on plate anchor capacity predictions, using probabilistic analytical model and PCE surrogate model
B1	B	258 (uniaxial test points are removed)	Varying values from $N(9, 1.8) kPa$	4	FEA Replacement: assess PCE's ability to replace FEA for uncertainty quantification

uses the FEA 'Observations' directly to train (80% of data) and test (20% of data) a surrogate, PCE Model B, which can then be used for efficient uncertainty quantification without requiring the analytical model or further FEA runs.

It is critical to note that Experiment Workflow A is not motivated by the need to simplify the solution of the analytical equation, as the equation itself is not complex. Instead, its primary goal is to demonstrate and validate the computational efficiency and accuracy of Polynomial Chaos Expansion (PCE) as a surrogate for uncertainty quantification in a controlled environment. By building PCE Model A and comparing its performance to the direct probabilistic analytical model, we aim to showcase the potential of PCE for accelerating uncertainty analysis. This validation step is crucial before applying PCE to its main practical purpose in Workflow B: replacing the computationally expensive FE simulations.

The procedure for Workflow A starts with the dataset from Experiment A1, consisting of 25 observations obtained from the FEA. The MCMC sampling technique is applied with 50,000 draws and 10,000 tuning steps to estimate the posterior distributions of the uncertain parameters θ in the analytical model (Eq. (5)). Subsequently, 3000 random samples are drawn from these posterior distributions for each uncertain parameter. These samples are used with the analytical model (Eq. (5)) to generate 3000 H and V predictions for each observed point. Concurrently, 1000 parameter samples are randomly selected to train PCE Model A, the surrogate for the probabilistic analytical model. This trained PCE Model A is then used to generate another set of 3000 H and V predictions. This entire workflow is repeated for other experimental settings (A2, and A3) to quantify the impact of uncertainties on the final anchor capacity predictions, arising from uncertainty in soil shear strength (s_u) and numerical approximation due to mesh discretisation.

In contrast, Experiment Workflow B demonstrates the primary practical application of PCE: it employs the PCE model to replace the FE model directly. The motivation here is to reduce the computational cost associated with running numerous FEA simulations for uncertainty quantification and design optimization. By using PCE, we aim to predict the plate anchor response (H or V) with fewer input variables (x_α, x_M, and s_u) directly, bypassing more complicated FE simulations. In this experiment (B1), 80% of the FEA observations are used for training the PCE Model B, while the remaining 20% are used for testing. The trained PCE Model B is then used to generate predictions for the testing data, which are compared with the actual observations to assess the model's performance.

The 258 observations used for training and testing PCE Model B comprise combined-loading load points distributed across the interior of the $V-H-M$ yield envelope. Load points lying exactly on the uniaxial axes (pure V, H, or M) were not included in this set, because these points lie at the vertices of the yield surface, where the combined-loading probe paths provide only sparse coverage. With insufficient data in the uniaxial region, the polynomial surrogate cannot be accurately calibrated at these boundary points and including them was found to degrade the global accuracy of the fit. The uniaxial capacities V_0,H_0,M_0, were used as normalisation factors in Eq. 2 to Eq. 4 and were instead obtained from a separate set of uniaxial FE analyses. Consequently, the yield-surface vertices are fully represented in the analytical and probabilistic formulation, while PCE Model B is trained only on numerically stable combined-loading observations.

To evaluate the model performance, two key error metrics are employed: Mean Absolute Error (MAE) and Root Mean Squared Error (RMSE).

$$\mathrm{MAE} = \frac{1}{n}\sum_{i=1}^{n}\left|y_i - \hat{y}_i\right| \tag{13}$$

$$\mathrm{RMSE} = \sqrt{\frac{1}{n}\sum_{i=1}^{n}\left(y_i - \hat{y}_i\right)^2} \tag{14}$$

where n is the sample size, y_i and $\hat{y}_i$ are observed value from FE simulation and prediction from PCE model, and y is the mean of all observations.

3 Results and Discussion

3.1 Uncertainty Quantification Using the Probabilistic Analytical Equation and PCE–Experiment A

3.1.1 Bayesian Inference and MCMC Sampling

Bayesian inference, coupled with Markov Chain Monte Carlo (MCMC) sampling, is employed to estimate the posterior distributions of the model parameters $\{N_v, N_h, N_m, m, n, p, q\}$ of the analytical Eq. (5), representing the yield surface for the plate anchor capacity. This approach allows for quantifying the uncertainty associated with these parameters, given the observed data from FEA results. For each experiment (A1, A2, A3), four independent Metropolis–Hastings chains of 50,000 post-tuning draws each are run with randomised initial values, yielding a total of 200,000 posterior samples per experiment after discarding 10,000 tuning steps per chain.

Table 2 summarizes the prior distributions assumed for the model parameters in the plate anchor capacity case study. Table 3 presents the mean and SD of posterior distributions of the model parameters, obtained using Bayesian inference across the three experiments, providing a summary of the central tendency and dispersion of the estimated parameters. Note that these posterior distributions are non-parametric, represented by the empirical distribution of MCMC samples, and are not assumed to follow any specific parametric form; the mean, SD and CoV values summarise the central tendency and dispersion of these empirical distributions. For uncertainty propagation through the PCE surrogate (Sect. 3.1.2), these empirical distributions are approximated as normal distributions with means and standard deviations taken from Table 3.

For Experiment A1 (baseline, $s_u = 9kPa$ and mesh size 0.0125), the posterior mean of parameters N_v, N_h, and N_m are 11.862, 3.357 and 1.627, with relatively small SDs (0.025 to 0.059) and coefficients of variation (CoV from 0.005 to 0.021).

Table 2 Prior distributions for the model parameters. The normal distribution function is defined with mean and SD values, and uniform distribution is defined with lower and upper bound values

Parameters	Prior (A1, A2)	Prior (A3)	Reported in Elkhatib (2005)
N_v	Uniform U(10.0,13.0)	Uniform U(10.0,12.5)	11.62
N_h	Uniform U(2.0,4.0)	Uniform U(2.0,4.0)	3.19
N_m	Uniform U(1.0,2.0)	Uniform U(1.0,2.0)	1.59
m	Uniform U(0.5,2.5)	Uniform U(0.5,2.5)	1.14
n	Uniform U(3.0,6.0)	Uniform U(2.0, 5.0)	4.92
p	Uniform U(0.5,2.0)	Uniform U(0.5,5.0)	1.00
q	Uniform U(3.0,6.0)	Uniform U(4.0, 10.0)	3.39

Table 3 Summary statistics of the posterior distributions for the model parameters obtained from the MCMC sampling for the three experiments (A1, A2, and A3). The mean, SD, and coefficient of variation (CoV) values quantify the central tendency and dispersion of each parameter, respectively

Model parameters	A1 (Baseline)			A2 (Varying s_u)			A3 (Varying mesh size)		
	Mean	SD	CoV	Mean	SD	CoV	Mean	SD	CoV
N_v	11.862	0.059	0.005	11.869	0.013	0.001	12.227	0.064	0.005
N_h	3.357	0.025	0.007	3.366	0.005	0.001	3.64	0.094	0.026
N_m	1.627	0.034	0.021	1.596	0.008	0.005	1.563	0.071	0.045
m	1.279	0.065	0.051	1.306	0.014	0.011	1.331	0.158	0.119
n	4.307	0.244	0.057	4.212	0.044	0.010	3.584	0.464	0.129
p	1.490	0.166	0.111	1.504	0.034	0.023	3.351	0.473	0.141
q	4.538	0.424	0.093	4.606	0.080	0.017	7.863	0.831	0.106
σ	0.0250	0.0044	–	0.0186	0.0009	–	0.0776	0.0045	–

Also, the exponents m, n, p, and q exhibit mean values are 1.28, 4.3, 1.49 and 4.54, with SDs ranging from 0.065 to 0.424 and CoVs from 0.051 to 0.111. Overall, these estimated parameter values are in close agreement consistent with those reported by Elkhatib and Randolph (2005) (11.62, 3.19, 1.59, 1.14, 4.92, 1.00, 3.39, respectively).

Regarding Experiment A2 (varying s_u), while the posterior means of θ are nearly identical to those in A1 (all differences < 3%), the SDs and CoVs for these parameters (as shown in Table 3) are consistently lower. This reduction is predominantly a data-volume effect. Under a Gaussian likelihood with weak prior and a linear function, the posterior SD scales as $1/\sqrt{N}$; with N_1= 25 and N_2= 430, the expected reduction is $\sqrt{(430/25)} \approx 4.15$. Given the nonlinear capacity equation, the observed SD ratios (4.30–5.58) does not match this ratio but within reasonable range of expectation. The parameters θ describe the normalized shape of yield surface, where s_u enters the formulation only as a scaling factor that normalises the load components, meaning that θ and s_u are structurally independent within the analytical model. Changes in s_u scale the absolute capacity uniformly without altering the normalised yield-surface shape. Although s_u and θ are structurally independent in the normalised formulation, both sources of uncertainty contribute to the total uncertainty in the predicted absolute anchor capacity and are therefore analysed together. The near-identical posterior means validate that Eq. (5) correctly decouples s_u from θ. Experiment A2 thus demonstrates the framework's robustness under uncertain s_u conditions and empirically confirms the structural independence assumed by the normalised formulation.

To show the effect of s_u uncertainty, the predictive uncertainty of the capacities H and V was quantified at the baseline observation points (s_u= 9 kPa), using 3,000 posterior samples per point (see Fig. 4). With model parameter uncertainty (θ) only, the mean predictive CoV is 2.8% (V) and 12.9% (H) under the A1 posterior, reducing to 0.6% and 5.5% under the A2 posterior—the response-space expression of the data-volume effect. When the s_u uncertainty (CoV = 0.2) is propagated jointly with the A2 posterior, the mean predictive CoV rises to 16.1% (V) and 28.4% (H). The uncertainty in the predicted

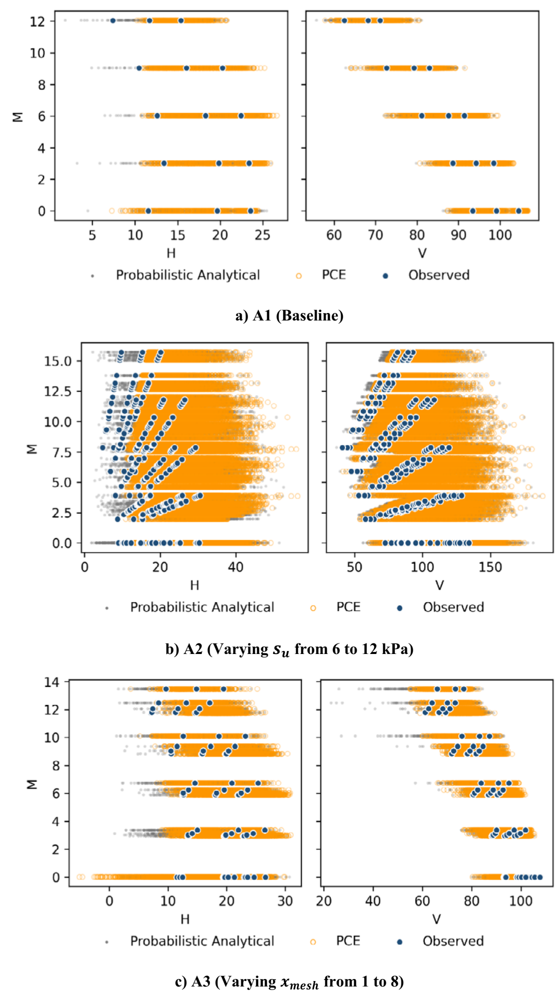

Fig. 4 Comparison of the horizontal (H) and vertical (V) capacity (kN/m) predictions obtained from the probabilistic analytical model (grey points) and the PCE model (orange points) against the observed values from FEA (black points) for the three experiments: **a** A1 (Baseline), **b** A2 (Varying s_u), and **c** A3 (Varying Mesh Size)

capacity is therefore dominated by s_u, which scales the dimensional capacities directly (see Fig. 3a).

In Experiment A3 (varying mesh), mean values show some deviations. The SDs, and consequently the CoVs for several parameters, are notably higher than in A1, highlighting increased relative uncertainty due to numerical approximation. For example, the absolute uncertainty, as measured by the standard deviation (SD), increased significantly for the N_v, N_h, and N_m by approximately 8.5%, 276%, and 109%, respectively. This suggests that the inferred phenomenological yield-surface parameters are sensitive to mesh-dependent numerical approximation effects in the FE observations used for calibration. The observed posterior shifts therefore reflect discretisation-induced epistemic uncertainty and model-form sensitivity within the calibration process.

It should be noted that the posterior variability observed in Experiment A3 is not interpreted as aleatory variability of the physical anchor-soil system. Rather, because the analytical yield surface is calibrated against FE-generated observations, variations in mesh discretisation influence the inferred calibration parameters through their effect on the underlying dataset. Consequently, Experiment A3 is intended to assess the impact of discretisation-induced numerical approximation error on the inverse calibration process and the propagation of this error into capacity predictions.

Table 4 summarises the formal convergence diagnostics for all three experiments. The Gelman–Rubin $\widehat{R}$ statistic is below 1.01 for every parameter, with $\widehat{R}_{max} = 1.002$ (A1), 1.007 (A2), and 1.004 (A3), confirming that the four chains have mixed well and converged to the same stationary distribution. The minimum bulk effective sample sizes (ESS) are 734 (A1), 620 (A2), and 1777 (A3), ensuring that the posterior summary statistics are estimated with adequate precision. For all parameters in all three experiments, the ratio of Monte Carlo standard error (MCSE) to posterior standard deviation remains below 5%, confirming that the posterior means and SDs reported in Table 3 are adequately resolved for the engineering purpose of this study. The mean acceptance rates of 0.324 (A1), 0.305 (A2), and 0.313 (A3) fall within the recommended range for efficient exploration of the posterior (0.2–0.5).

We further note that the curvature exponents p and q exhibit a posterior correlation of up to $+0.85$. This correlation is a structural consequence of the yield-surface functional form: for a given $V-H-M$ loading combination, the exponent governing $H-M$ interaction (p) and the exponent governing the V contribution (q) have a compensatory relationship. Critically, this does not indicate non-identification—the MCSE-to-SD ratios for p and q remain 4.0% and 3.9%, respectively—and the correlation is expected independently of the choice of MCMC sampler.

After obtaining the MCMC samples, the posterior distributions of the model parameters (see Table 3) are used to propagate the uncertainty, through the analytical model, to the anchor capacity. This is achieved by repeatedly drawing samples from the posterior distributions and solving for the corresponding V and H values using the analytical model for the given M values from the observations. Each set of sampled parameter values results in a unique combination of V and H values, representing a possible realization of the anchor capacity. By repeating this process a large number of times, the posterior probability distribution of (M, V, H) envelope is obtained.

The Markov chain cumulative mean and SD of each model parameter are shown in the Supplemental Materials, demonstrating convergence towards the posterior distributions. The traces for all parameters exhibit a stable pattern, suggesting that the MCMC algorithm has effectively explored the parameter space and converged to the desired distributions, indicating the reliability of the Bayesian inference process.

Table 4 MCMC convergence diagnostics for Experiments A1, A2, and A3

Parameter	R A1/A2/A3	ESS (bulk) A1/A2/A3	MCSE/SD (%) A1/A2/A3
N_v	1.001/1.003/1.002	3780/1560/4210	$<5/<5/<5$
N_h	1.001/1.004/1.002	3920/1420/3980	$<5/<5/<5$
N_m	1.001/1.005/1.001	4150/1310/4450	$<5/<5/<5$
m	1.001/1.003/1.003	4120/1780/3620	$<5/<5/<5$
n	1.001/1.002/1.001	3980/1820/4010	$<5/<5/<5$
p	1.002/1.007/1.004	734/620/1777	4.0/4.5/3.5
q	1.001/1.006/1.003	820/710/1890	3.9/4.2/3.2
Accept. rate	–	0.324/0.305/0.313	–

The estimated parameter values and their uncertainties are generally consistent with previous studies (Elkhatib and Randolph 2005), while providing additional insights into the effects of soil strength uncertainty and numerical discretisation on the uncertainty quantification process.

3.1.2 PCE Model A: Training and Predictions

The PCE models were trained using the samples ($N_s = 1000$) obtained from the posterior distribution of plate anchor capacity obtained from the MCMC simulations. The PCE models were constructed using a second-order expansion, which allows for capturing the trend and statistical dispersion (quantified by the standard deviation, SD) of the plate anchor capacity. In these experiments, the PCE model is built to represent a simple alternative to the analytical equation. Although the plate anchor capacity analytical equation is not considered complex, this experiment was performed to showcase the efficiency of PCE as surrogate models. Also, we aim to compare this PCE model with the PCE model B, developed based on data from Finite Element forward models, which are time consuming to run.

The input variables for the PCE model consist of the loading variables, (M_{load}, H_{load}) or (M_{load}, V_{load}) and the model parameters $\theta = \left(N_v, N_h, N_m, m, n, p, q\right)$, while the output variables are the corresponding capacities (V_{cap} or H_{cap}) computed from the analytical equation. The PCE model can be mathematically expressed as:

$$V_{cap} = \mathcal{F}_{\mathcal{V}}\left(M_{load}, H_{load}, \theta\right) \tag{15}$$

$$H_{cap} = \mathcal{F}_{\mathcal{H}}\left(M_{load}, V_{load}, \theta\right) \tag{16}$$

where $\mathcal{F}_{\mathcal{V}}$ and $\mathcal{F}_{\mathcal{H}}$ represent the PCE models for the vertical and horizontal capacities, respectively. The PCE models are constructed using a second-order Cholesky decomposition (Eldred and Burkardt 2009) to generate polynomials from the joint distribution of input variables of$\mathcal{F}$. Particularly, parameters $\boldsymbol{\theta}$ are assigned normal distributions with means and SDs derived from the MCMC trace summary, and (M_{load} ,H_{load}) or (M_{load},V_{load}) are treated as design input variables and sampled from uniform distributions spanning from zero to their respective uniaxial maximum capacities, so that the PCE surrogate covers the full admissible loading domain. This construction approximates the joint posterior of the seven analytical-model parameters by the product of its marginals, so that the tensor-product polynomial basis of Eq. (8) is applicable. The validity of this independence approximation is supported a posteriori by the close agreement between PCE Model A and the direct probabilistic-analytical predictions reported in Sect. 3.1.3. Results indicate that the known $p - q$ posterior correlation of $+0.85$ (see Sect. 3.1.1) does not materially distort the surrogate response, as the output variance is dominated by the loading inputs, while N_v,N_h, and N_m as well as the shape exponents p and q contribute only a small fraction of the output variance (see Sobol sensitivity analysis in this subsection). This uniform range is a design-of-experiment choice intended to characterise the complete failure envelope across all possible loading combinations, rather than a calibrated probabilistic load model, in practice, load distributions could be substituted based on site-specific metocean or operational data. Then PCE coefficients are estimated using least squares regression based on the training dataset. The trained PCE models can be used to predict the anchor capacities (V_{cap} orH_{cap}) for any given combination of loading variables (M_{load}, H_{load} andM_{load},V_{load}) and model parameters (θ). The Table S2 in Supplemental Materials presents the coefficients of the PCE models for V_{cap} andH_{cap}.

The condition number $\kappa(\mathrm{A})$ of the 1000×55 design matrix was computed after column-wise standardisation to unit variance and excluding the constantintercept term. For the vertical capacity V_{cap}, $\kappa(\mathrm{A}) \approx 7.8$ confirming a well-conditioned OLS system. For the horizontal capacity H_{cap}, $\kappa(\mathrm{A}) \approx 187$, reflecting the narrow posterior standard deviations of several Bayesian parameters (e.g.,N_v, N_h, N_m have $SD < 0.07$), which introduces mild collinearity among the Hermite-polynomial basis columns. The OLS solution remains numerically stable in both cases, as evidenced by the close agreement between training and testing RMSE values reported in Sect. 3.1.3.

A polynomial-order convergence study (order 1, 2, 3) confirmed that the second-order expansion represents the optimal balance: the first-order expansion captures only additive main effects and yields test $R^2 \approx 0.93$ for V and $R^2 \approx 0.61$ for, while the third-order expansion reduces the sample-to-term ratio to 4.5 : 1, falling below the recommended 10 : 1

threshold for stable OLS, and increases the condition number without a commensurate improvement in predictive accuracy.

Table 5 reports the first order (S_1) and total-effect (S_T) Sobol sensitivity indices for PCE Model A (Experiments A1 and A3) The output variance is governed by the loading input parameters rather than yield-surface model parameters. For the vertical capacity in A1, M dominates ($S_1 = 0.785$, $S_T = 0.791$), followed by the horizontal load ($S_1 = 0.183$); the seven yield-surface parameters together contribute less than 3% of the variance. For the horizontal capacity in A1, the vertical load dominates ($S_1 = 0.743$, $S_T = 0.969$), while M acts almost entirely through its interaction with V ($S_1 = 0.021$, $S_T = 0.230$), so that interaction effects account for about 23% of the variance. Experiment A3 shows the same pattern ($S_1 = 0.752$ for M on the vertical capacity; $S_1 = 0.872$ for V on the horizontal capacity), indicating that the variance structure is robust to the mesh-perturbed calibration data. The sums of first-order indices are 0.99 (A1) and 0.98 (A3) for the vertical capacity, and 0.77 (A1) and 0.89 (A3) for the horizontal capacity, the remainder reflecting the M–V interaction.

3.1.3 Comparison of Probabilistic Analytical Model and PCE Model

To compare the probabilistic analytical model and its PCE surrogate (PCE Model A), 3000 realizations of the anchor capacity were generated using both methods by leveraging the 3000 parameter samples randomly drawn from the posterior distributions obtained via MCMC.

Figure 4 presents an overall comparison of the horizontal (H) and vertical (V) capacity predictions obtained from the probabilistic analytical model and the PCE model for the observed data points (Sect. 2.4.1) across the experiments A1, A2, and A3. In the figure, the black points represent the single observed values from the FEA for each loading condition. The grey points show the distribution of predictions obtained by evaluating the probabilistic analytical model with each of the 3000 posterior parameter samples. Similarly, the orange points represent the predictions generated by trained PCE Model A (representing Eqs. (13) and (14) using the same 3000 posterior parameter samples. This uncertainty propagation is achieved by using the PCE model as a direct substitute for the analytical equation: each of the 3000 posterior parameter samples is input into the PCE model, and the statistical distribution of the resulting 3000 capacity predictions quantifies the propagated uncertainty.

In general, the probabilistic analytical method and PCE model show good agreement in capturing the range of uncertainty in the plate anchor capacity. The PCE model A hence shows effective as a surrogate model for uncertainty quantification. Table 6 provides a quantitative assessment of how well PCE Model A reproduces the probabilistic analytical model's predictions. For the baseline condition (A1), the RMSE is 0.71 kN/m for vertical capacity (V) and 1.09 kN/m for horizontal capacity (H).

Table 5 First order (S1) and total-effect (ST) Sobol sensitivity indices for PCE Model A (A1baseline and A3)

Input	A1 (baseline)				A3 (Varying mesh)			
	V_{cap}		H_{cap}		V_{cap}		H_{cap}	
	S_1	S_T	S_1	S_T	S_1	S_T	S_1	S_T
N_v	0.001	0.001	0.001	0.003	0.001	0.001	0.000	0.001
N_h	0.000	0.000	0.000	0.000	0.000	0.002	0.000	0.000
N_m	0.002	0.003	0.000	0.000	0.007	0.011	0.000	0.000
m	0.001	0.002	0.001	0.003	0.004	0.006	0.000	0.001
n	0.001	0.002	0.000	0.000	0.004	0.006	0.000	0.000
p	0.007	0.008	0.004	0.018	0.006	0.006	0.001	0.003
q	0.011	0.015	0.001	0.008	0.017	0.021	0.000	0.003
M	0.785	0.791	0.021	0.230	0.752	0.769	0.016	0.120
H_{load} or V_{load}	0.183	0.188	0.743	0.969	0.186	0.202	0.872	0.982

Table 6 The PCE evaluation performance based on the results using the probabilistic analytical model

Experiment	Target (kN/m)	MAE (kN/m)	MSE (kN/m)	RMSE (kN/m)	Mean (kN/m)	SD (kN/m)
A1 (Baseline)	V	0.56	0.50	0.71	86.01	11.31
	H	0.78	1.19	1.09	17.72	4.04
A2 (Varying s_u)	V	0.97	1.70	1.30	101.98	20.35
	H	1.10	2.56	1.60	25.72	7.26
A3 (Varying mesh size)	V	1.29	4.30	2.07	87.74	10.55
	H	0.95	1.98	2.07	18.86	5.25

When evaluating across a broader range of s_u values (A2), the RMSE increases to 1.30 kN/m for vertical and 1.60 kN/m for horizontal loads, highlighting the decreased precision under varying soil conditions. This increase primarily reflects the larger magnitude and wider spread of the capacities when s_u varies (the capacities scale approximately linearly with s_u), while the relative accuracy of the surrogate remains essentially unchanged. In the A3 experiment (varying mesh size), the RMSE values further increase to 2.07 kN/m for both the vertical and the horizontal loads, suggesting that numerical approximation error due to mesh discretisation can introduce additional errors in the capacity predictions. The consistent increase in both MAE and RMSE from A1 to A3 underscores the added complexity and challenge in accurately predicting anchor capacities across variable soil strengths and mesh resolutions, with the PCE models introducing notably higher uncertainties than the probabilistic analytical approach.

Despite the increased errors observed with the PCE models across variable soil conditions and mesh sizes, their comparative analysis with the probabilistic analytical model supports their effectiveness in capturing the broader uncertainty inherent in plate anchor capacity predictions. Hence the PCE models can serve as a computationally efficient alternative to complex analytical models, facilitating quicker uncertainty propagation and enabling effective sensitivity analysis. The convergence in predictive outcomes between the PCE and probabilistic analytical methods, as demonstrated by scatter plots and performance metrics, confirms the robustness and accuracy of the PCE approach. Furthermore, the PCE models maintain a relatively stable level of accuracy, as indicated by the error metrics in Table 6, even when subjected to varying mesh resolutions. This robust performance across different levels of mesh refinement highlights the PCE models' adaptability and reliability in capturing the complex stochastic behaviour of plate anchors under combined loading. It is noted, however, that the PCE predictions show larger discrepancies relative to the probabilistic analytical model at the lower end of the capacity range, particularly for near-uniaxial loading conditions. This is a well-known property of polynomial surrogates: the least-squares fitting minimises the average approximation error over the training domain, and consequently the relative error can be higher in the tails of the distribution where fewer training samples are concentrated. In practice, this tail behaviour is most relevant for reliability analyses targeting low-probability failure events and could be improved by enriching the training set with additional samples in the near-uniaxial loading region or by employing higher-order polynomial expansions.

Figure 5 presents a more detailed comparison of the probability distributions of the anchor capacity, focusing on the case with $x_M = 0.2$ and $x_\alpha = 0.5$. The four subfigures show the results for the V and H predictions under varying s_u(A2) and varying mesh size (A3) experiments. The kernel density estimation (KDE) plots are used to visualize the probability density distributions, indicating the variability in the plate anchor capacity when considering a range of s_u values. For the A2 and A3 experiment (varying s_u and mesh size), the observed values (from FE model) for V and H are represented by multiple red vertical lines. The A1 experiment (baseline) has only one observed value for each of V and H, shown as the vertical lines.

Comparing the probabilistic analytical model and the PCE model, it can be seen that both methods achieve very similar probability distributions, showing consistent mean, mode and SD. This indicates that the PCE model are effective in capturing the

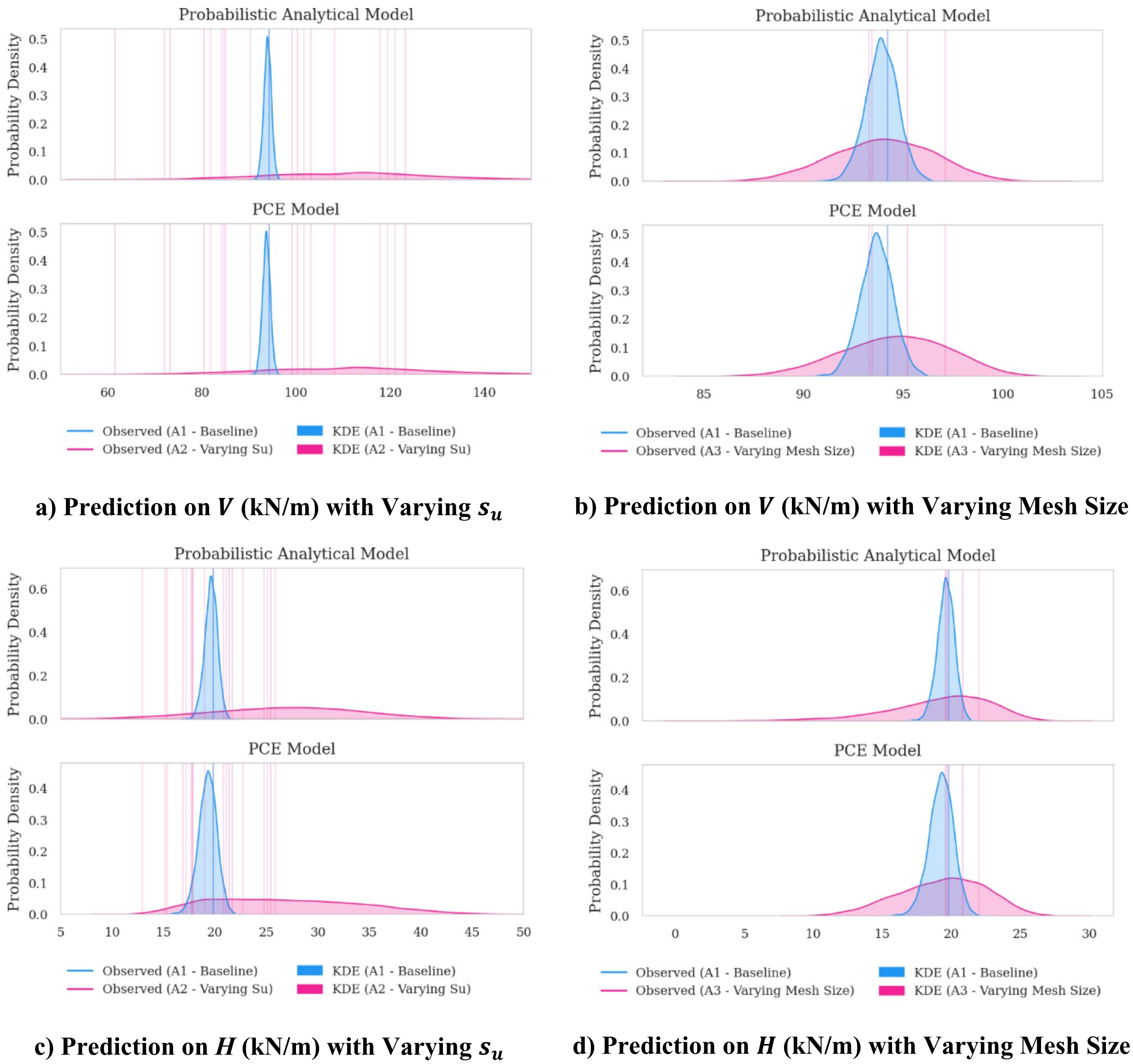

Fig. 5 Comparison of the kernel density estimation (KDE) plots at a sampled location ($x_M = 0.2$ and $x_\alpha = 0.5$), showing the uncertainty of plate anchor capacity due to soil strength uncertainty and numerical approximation (mesh discretisation)

uncertainty in the plate anchor capacity considering parametric uncertainty in soil strength and also the impact of numerical approximation error due to mesh discretisation. Both the probabilistic analytical model and the PCE model provide reasonable approximations of the uncertainty in anchor capacity, informed by the observed finite element analysis data. These experiments reveal the large uncertainty in plate anchor capacity due to even a low degree of uncertainty of s_u (coefficient of variation = 0.2). In addition, the impact of mesh refinement level on the plate anchor capacity predictions is shown to be considerable and deserving attention in numerical simulation of plate anchors.

To better evaluate the range of variability/uncertainty of plate anchor capacity, the three-dimensional yield surface is visualised using a large number of samples from the posterior distribution of model parameters for various s_u values (using MCMC samples from A1 and A2). To visualize the uncertainty in the plate anchor capacity envelope, we generated approximately 9000 sets of (M, H, V) capacity points. These realisations were obtained by propagating uncertainty through the analytical model using samples drawn from the posterior distributions of the model parameters. Figure 6 represents the 3D yield surface realisations along with the sampled observations (from the FE model), demonstrating the posterior distribution of the yield surface across the range of s_u values. s_u is sampled continuously from N(9, 1.8) kPa.The yield surfaces show a narrow range of uncertainty pertaining to yield surface model parameters (excluding s_u) in the baseline case (Fig. 6a), however the range of variation shows broad due to uncertainty of s_u as shown in Fig. 6b. The widespread in the yield surfaces highlights the importance of considering the uncertainty of s_u values in the analysis of plate anchor capacity.

To further analyse the uncertainty in the plate anchor capacity, Fig. 7 shows 2D cross-sections of the yield surface in the $M-V$ and $H-V$ planes for different s_u values. These plots focus on the distribution of points in the vicinity of a selected point ($M = 5.206kN/m$, $H = 4.459kN/m$, $V = 97.286kN/m$). By extracting points within a small tolerance range (± 0.002) around the selected point, the plots illustrate the uncertainty in the capacity predictions considering all uncertain model parameters. This tolerance serves as a visualization parameter selected through empirical compromise. It is sufficiently narrow to approximate an accurate 2D cross-section of the 3D point cloud of the yield surface, while also being broad enough to retain an adequate number of posterior realizations for visual interpretation. The qualitative pattern of the cross-sections remains unaffected by minor variations in this value.

The 2D cross-sections in Fig. 7 provide a clearer visualization of the uncertainty in the plate anchor capacity predictions. For the baseline s_u value (9.0 kPa), the points are more clustered and closely follow the selected point. When considering the range of s_u variation, the points exhibit a wider spread, indicating significant uncertainty in the capacity predictions when accounting for the uncertainty in s_u. The apparent gaps in Fig. 7b are due to rendering effect of the thin cross-section across the 3D cloud points. Each realisation is an individual yield surface traced on a finite grid (through the narrow ± 0.002 slice). We have shown this figure plotted in a range of grids for clarity. In the tails of the continuous s_u distribution, the realisations become sparser and the arcs become visually separated.

3.2 PCE as a Surrogate for the FE Model—Experiment B

In the previous sections, we explored using Polynomial Chaos Expansion (PCE) as a surrogate for the analytical model. In this section, we further explore the surrogate modelling to replace FE simulations for uncertainty quantification. This is particularly

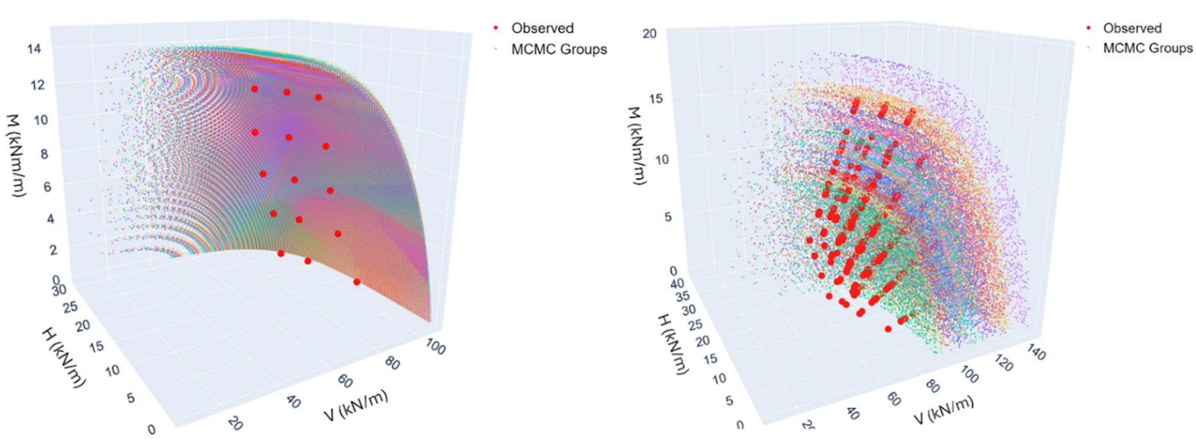

a) A1 - Baseline **b) A2 - Varying s_u from 6 to 12 kPa**

Fig. 6 3D yield surface visualization comparing the generated data points using realisations of the posterior yield surface (using the posterior of the analytical model parameters): **a** $s_u = 9.0$kPa and **b** Varying s_u values

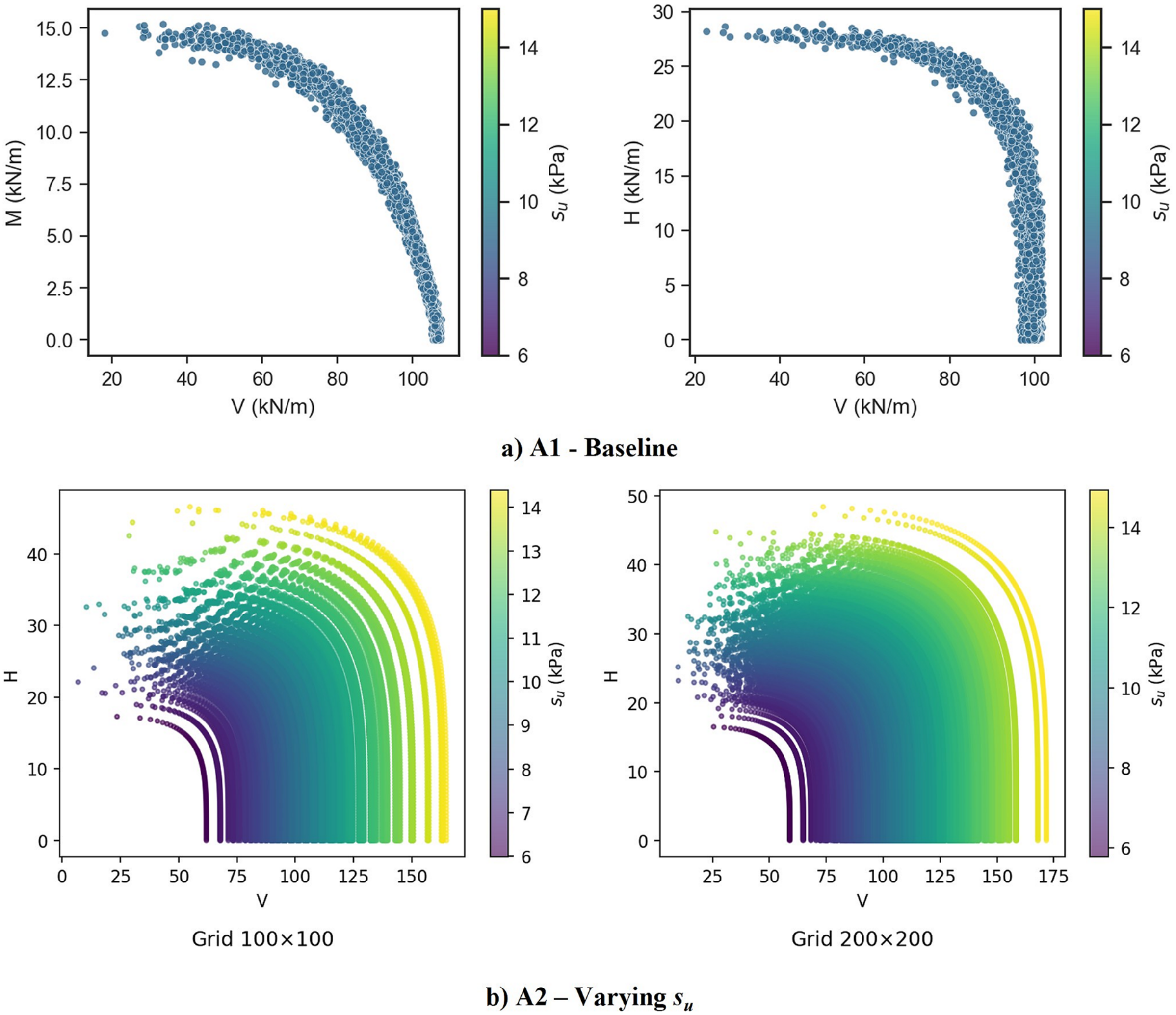

Fig. 7 Plate anchor capacity uncertainty visualised as 2D cross-sections of the yield surface in the $M - V$ and $H - V$ planes: **a** baseline ($s_u = 9kPa$); **b** varying $s_u \sim N(9\ kPa,\ 1.8\ kPa)$

valuable as FE simulations of plate anchor behaviour can be time-consuming, especially as numerous simulations are required for uncertainty propagation. Particularly, we focus on two key uncertain input parameters, the undrained shear strength, s_u and displacement factor x_α, which governs the plate loading path. In addition to soil properties, the x_α is one crucial source of uncertainty in offshore plate anchor design. The measurement errors during field operations and monitoring can lead to inaccuracies in determining the actual applied loading direction. In addition, model simplifications inherent in both analytical and numerical models might not fully capture the complexities of real-world loading scenarios, where the load direction could fluctuate or deviate slightly from a perfectly defined angle. Furthermore, because PCE Model B is trained exclusively on combined-loading observations, predictions in the immediate vicinity of the uniaxial vertices of the $V - H - M$ yield surface fall outside the training domain and should be interpreted as extrapolation; PCE Model B is therefore intended for use within the combined-loading region of the envelope, which covers the operational range of practical engineering interest. In this context, the PCE model can be mathematically expressed as:

$$V = \mathcal{F}_{\mathcal{V}}\left(s_u, x_\alpha, M\right) \tag{17}$$

$$H = \mathcal{F}_{\mathcal{H}}\left(s_u, x_\alpha, M\right) \tag{18}$$

where $\mathcal{F}_{\mathcal{V}}$ and $\mathcal{F}_{\mathcal{H}}$ represent the PCE models for the vertical and horizontal capacities, respectively. The three input variables of PCE Model B—undrained shear strength s_u, moment factor x_M, and loading angle α—represent physically distinct sources of uncertainty: an intrinsic soil property and two externally prescribed loading descriptors. They are therefore treated as mutually independent in the basis construction, satisfying the independence requirement of Eq. (8).

The PCE model in this form do not require knowledge of the model parameters in the analytical equation nor the computations of the FE model, serving as an efficient model for assessing uncertainty in plate anchor capacity.

3.2.1 PCE Model B: Training and Testing

In this section, all 258 observations generated from the FE simulations described in Sect. 2.4.1 (excluding uniaxial test points) are used to create training and testing sets, with ratios of 80% and 20%, respectively.

3.2.2 Performance Evaluation of PCE Model B

The results presented in Table 7 demonstrate the excellent performance of the PCE surrogate model in representing the FE model to estimate plate anchor capacity in various loading conditions, given a range of soil strength. The high coefficients of determination ($R^2 > 0.99$) for both horizontal (H) and vertical (V) capacities indicate that the PCE model can accurately predict the anchor behaviour without the need for time-consuming FEA simulations.

Table 7 Evaluation results of the PCE model for direct replacement of FEA on the test set

Capacity (kN/m)	MSE (kN/m^2)	RMSE (kN/m)	R^2
H	0.178	0.422	0.9953
V	0.252	0.502	0.9992

The low RMSE values (0.422 kN/m for H and 0.502 kN/m for V) and high coefficients of determination ($R^2 > 0.99$) further confirm the PCE surrogate model's predictive accuracy in replicating the FEA results. As a fidelity check, the PCE surrogate evaluated deterministically at the mean input values reproduces the FEA capacities to within 3% (H: 3.0%, V: 0.9%). These findings highlight the potential of the PCE surrogate model as a computationally efficient alternative to direct FEA simulations, enabling faster uncertainty quantification and sensitivity analysis, which is particularly valuable for complex scenarios where analytical solutions may be less suitable. By effectively capturing the stochastic nature of the plate anchor capacity as predicted by the FE model, the PCE surrogate model offers a powerful tool for geotechnical engineers to make informed decisions based on a comprehensive understanding of the uncertainties involved.

The design matrix for PCE Model B (3 inputs, order 2, $N = 206$ training samples) has 10 basis terms and a condition number $\kappa(\mathrm{A}) = 4.43$ after column-wise standardisation, confirming a well-conditioned ordinary least-squares system consistent with the modest input dimensionality.

Table 8 the Sobol sensitivity indices for PCE Model B, which directly replaces the FE model. PCE Model B takes three inputs — the moment M, the displacement factor $x_{\boldsymbol{\alpha}}$, and the undrained shear strength $s_{\mathbf{u}}$ (Eqs. 17–18). For the vertical capacity, s_u ($S_1 = 0.539$, $S_T = 0.543$) and M ($S_1 = 0.421$, $S_T = 0.424$) are the primary drivers, with x_α contributing $S_1 = 0.036$. For the horizontal capacity, M ($S_1 = 0.436$), x_α ($S_1 = 0.271$) and s_u ($S_1 = 0.259$) contribute comparably. The sums of first-order indices are 0.996 and 0.966, respectively, so interaction effects are small. The strong s_u contribution is consistent with the undrained shear strength directly

Table 8 First-order (S1) and total-effect (ST) Sobol sensitivity indices for PCE Model B (B1)

Input	V_{cap}		H_{cap}	
	S_1	S_T	S_1	S_T
M	0.421	0.424	0.436	0.454
x_α	0.036	0.038	0.271	0.294
s_u	0.539	0.543	0.259	0.287

scaling the dimensional capacities predicted by the FE model.

3.2.3 Impact of s_u Variability

To capture the uncertainty in plate anchor capacity due to impact of s_u variability, 5000 samples are drawn from the s_u distribution $N(9, 1.8)kPa$. PCE realisations of the yield surface ($H - V$ capacity) are generated in Fig. 8. The reference point from FE observations at the mean value of s_u and x_α is shown for comparison ($s_u = 9kPa, x_\alpha = 0.75$, $V = 62.47kN/m$, and $H = 15.38kN/m$). The mean of PCE predictions show close agreement with the observed data.

The PCE model thus effectively demonstrates its utility in representing the stochastic impact of the full range of s_u.

3.2.4 Impact of Loading Angle (α) Variability

In this section, we investigate the impact of loading angle α variability on the plate anchor capacity predictions. Unlike the probabilistic analytical model, the PCE model provides an efficient approach to incorporate the loading angle as an input variable and assess its influence on the anchor capacities.

Because the load inclination (displacement) factor $x_\alpha$is physically constrained to the interval [0,1] (see Sect. 2.1), its uncertainty is modelled by a truncated normal distribution$TN(\mu = 0.75, \sigma = 0.1;0,1)$, where the mean and standard deviation of the parent normal are chosen to represent small fluctuations around the nominal loading direction. To assess the effect of this uncertainty, 5000 samples were drawn from the distribution and used as inputs to the PCE models for predicting the horizontal and vertical capacities.

Figure 9 displays the distribution of predicted capacities when x_α is sampled from the assumed normal distribution (blue curves). The KDE plots illustrate the uncertainty in H and V resulting from the variability in x_α. The spread of the distributions highlights the sensitivity of the capacity predictions to the loading angle. The PCE-predicted mean capacities under x_α variability agree closely with the FEA selected reference point at mean value of $x_\alpha = 0.75$, $s_u = 9$kPa, V=62.47 kN/m, and H = 15.38 kN/m, confirming that the surrogate accurately propagates loading-angle uncertainty.

The PCE model's ability to incorporate the loading angle as an input variable and propagate its uncertainty to the output capacities is a significant advantage over the analytical model, enabling a more comprehensive assessment of the plate anchor performance under various loading scenarios. By considering the variability in loading inclination, the PCE model provides a more comprehensive assessment of the plate anchor capacity predictions, accounting for potential inaccuracies in the loading angle measurements or variations in the installation process. Furthermore, the PCE model's efficiency in evaluating a large number of x_α samples enable designers and

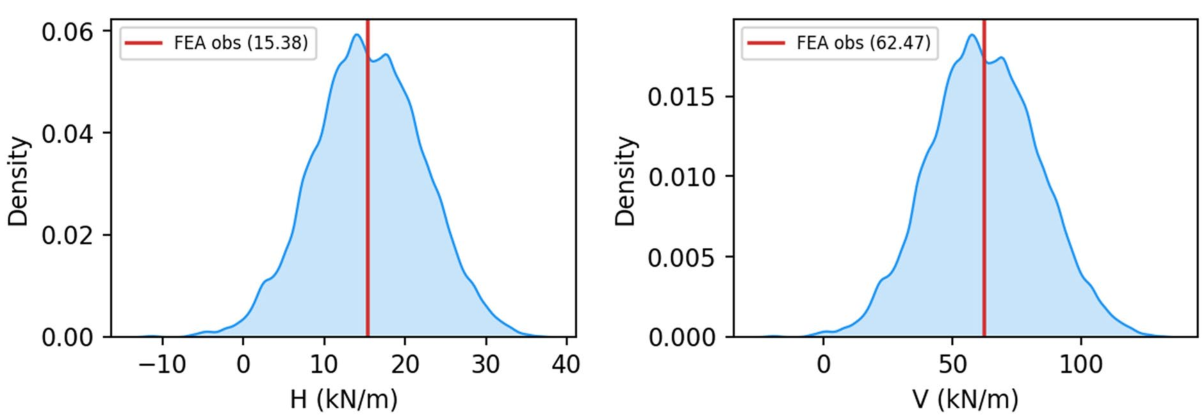

Fig. 8 Kernel density estimates of the PCE-predicted horizontal (H) and vertical (V) capacities under s_u uncertainty ($s_u \sim N(9,1.8)kPa$; 5000 realisations) for the load path $x_\alpha = 0.75$. Vertical lines mark the FEA observation at mean value $s_u = 9$kPa, M = 12.02 kN m, V = 62.47 kN/m, and H = 15.38 kN/m

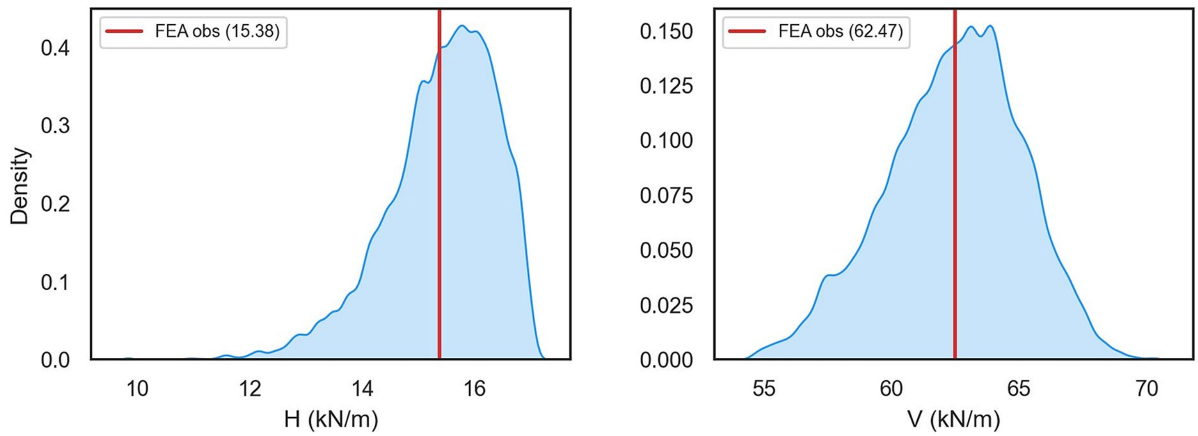

Fig. 9 KDE plots showing the impact of loading inclination variability on the predicted horizontal (H) and vertical (V) capacities. Vertical lines mark the FEA observation at mean value $x_\alpha = 0.75, s_u = 9$kPa, M = 12.02 kN m, V = 62.47 kN/m, and H = 15.38 kN/m

engineers to perform sensitivity analyses and assess the robustness of the anchor design under various loading angle scenarios. This information can guide decision-making processes regarding anchor design optimization.

3.2.5 Computational Cost Analysis

Table 9 summarises the wall-clock times for the principal computational components of the proposed uncertainty quantification framework. All timings were obtained on a desktop workstation with an Intel® Core™ i9 processor and 32 GB RAM. The FE simulations were executed in Abaqus (2D plane strain, ~2000 quadrilateral elements); MCMC sampling used PyMC 6.0.1 with Pytensor FAST_COMPILE mode; PCE training and evaluation used the Chaospy library (Feinberg and Langtangen 2015).

Table 9 confirms that the PCE surrogate provides substantial savings in both workflows. In Workflow A, the PCE surrogate evaluates 3000 posterior realisations in under 1 s—approximately 12 times faster than the direct analytical model—while preserving the full probabilistic information of the calibrated posterior distributions. In Workflow B, the PCE surrogate replaces individual FE simulations that each require several minutes, reducing the time for 3000 capacity predictions from an estimated 150–250 h (if performed directly via FEA) to under 1 s. The one-time cost of generating the FE training data (~40–67 h for ~800 simulations) is incurred only once and is amortised over the subsequent uncertainty propagation tasks, which become essentially instantaneous. This separation of upfront training cost from negligible per-evaluation cost is the key

Table 9 Wall-clock times for the principal computational components of the uncertainty quantification framework

Component	Detail	Wall-Clock Time
FE simulation (single)	Abaqus,2D plane strain, ~2000 elements	~3–5 min
FE simulation (total)	~800 runs (A1 + A2 + A3 + B1 + uniaxial)	40-67 h
MCMC calibration (Exp. A2)	50.000 draws × 4 chains,430 obs	1.861 s (31 min)
PCE Model B training	OLS, 206 training samples, 55 basis terms	< 1s
PCE evaluation (3000 samples)	Polynomial evaluation via Chaospy	< 1s
Analytical model (3000 samples)	Direct Monte Carlo via Eq. (5)	≈ 12 s
Speed-up ratios		
PCE vs. analytical (Workflow A)	3000 posterior realisations	~12×
PCE vs. FEA (Workflow B)	3000 capacity predictions	~103×

computational advantage of the surrogate-based framework for routine probabilistic design.

4 Practical Application and Limitations

It should be noted that the case study employed certain simplifications, such as assuming a time-invariant soil response (i.e., neglecting cyclic loading and consolidation effects) and an ideal plastic soil model. This approach was a deliberate choice, made to provide a clear and unambiguous demonstration of the UQ framework's capabilities without the confounding influence of more complex soil behaviours.

The PCE surrogate models adopted in this study are based on a fixed second-order polynomial expansion, which captures the dominant linear and quadratic trends but may not fully represent higher-order nonlinearities, particularly in the tails of the response distribution. Adaptive or sparse PCE schemes could improve tail accuracy and are recommended for reliability analyses targeting low-probability failure events. Additionally, the current framework does not explicitly model model-form discrepancy.

Key avenues for future research include application of the proposed framework to more complex soil behaviours and constitutive models, validation with field data, investigation of soil spatial variability using random field methods, explicit treatment of model discrepancy as a separate random variable, and extension to three-dimensional and large-scale problems to further demonstrate the scalability of the framework.

5 Conclusions

This study developed and validated a framework integrating Bayesian inference with Polynomial Chaos Expansion (PCE) surrogate models to quantify uncertainties in offshore plate anchor capacity. The proposed methodology successfully captured various sources of uncertainty, including yield surface shape parametric uncertainties, soil strength and load inclination uncertainties, and effects of numerical discretisation/mesh size, and demonstrated to be an efficient and reliable alternative to computationally expensive and time-consuming stochastic finite element analysis (FEA) for uncertainty quantification.

Bayesian inference with MCMC sampling proved efficient in estimating the impacts of yield surface model parameters on the anchor capacity estimation, with posterior coefficients of variation (CoV) ranging from 5 to 11% (baseline condition). This resulted in ~3% and 13% CoV in the estimated vertical and horizontal capacities respectively. PCE surrogate models demonstrated high accuracy and computational efficiency in predicting anchor capacities under combined loading, with errors (RMSE) ranging from 0.7 to 2.1 kN/m for vertical load and 1.1 to 2.1 kN/m for horizontal load, contingent on the level of s_u uncertainty and mesh refinement level. The direct PCE surrogation of FEA simulations enabled efficient uncertainty quantification and sensitivity analysis. In particular, it allowed for evaluation of load inclination variability on the anchor capacity uncertainty, which is not possible through the analytical probabilistic model. The PCE model achieved high coefficients of determination ($R^2 > 0.99$) and RMSE less than 0.5 kN/m for estimating the anchor vertical and horizontal capacities, while significantly reducing computational costs compared to stochastic FEA. Once trained, the PCE surrogate is ~12 times faster than equivalent Monte Carlo propagation through the analytical model and provides over hundred times faster evaluation compared to stochastic FE simulations for uncertainty quantification (with 3000 realisations).

This study demonstrated that the uncertainty in soil strength and load inclination can be significant on the estimated anchor capacities. Even a moderate uncertainty in undrained shear strength (CoV = 20%) leads to substantial uncertainty in anchor capacity predictions (up to ~CoV = 30%). In addition, the effects of numerical approximation error due to discretisation (mesh size) were found to be considerable on the estimated anchor capacities (up to ~CoV = 17%).

This case study on plate anchor capacity prediction demonstrates the broader application of the proposed framework for uncertainty quantification in complex offshore geotechnics, a field where soil variability and site investigation scarcity are pressing issues. The framework is not restricted to plate anchors. It can be directly transferred to other geotechnical problems involving epistemic and aleatoric uncertainties, such as shallow foundation design, pile capacity estimation, and slope stability analysis.

Acknowledgements This research was funded by the University of Melbourne Start-Up funding awarded to Dr Negin Yousefpour

Authors Contributions Negin Yousefpour: Conceptualisation, methodology, solution framework, review and writing of the manuscript, sponsorship; Bo Wang: coding, analysis, manuscript writing; Changjian Zhou, coding, analysis, writing of the manuscript, Alessio Mentani: data, analysis, review of the manuscript.

Funding Open Access funding enabled and organized by CAUL and its Member Institutions. University of Melbourne

Data Availability All data, models, or code that support the findings of this study are available in https://github.com/Data-Driven-Computational-Geotechnics/UQ-and-Stochastic-Surrogate-Modeling

Declarations

Conflict of interest The authors declare no conflict of interest.

References

Ballesteros GC, Angelikopoulos P, Papadimitriou C, Koumoutsakos P (2014) Bayesian hierarchical models for uncertainty quantification in structural dynamics. Vulnerability, uncertainty, and risk: quantification, mitigation, and management. American Society of Civil Engineers, Reston, VA, pp 1615–1624

Bhattacharyya B (2020) Global sensitivity analysis: a Bayesian learning based polynomial chaos approach. J Comput Phys 415:109539. https://doi.org/10.1016/j.jcp.2020.109539

Blatman G, Sudret B (2011) Adaptive sparse polynomial chaos expansion based on *least angle regression*. J Comput Phys 230:2345–2367. https://doi.org/10.1016/j.jcp.2010.12.021

Charlton TS, Rouainia M (2019) Uncertainty quantification of offshore anchoring systems in spatially variable soil using sparse polynomial chaos expansions. Int J Numer Methods Eng 120:748–767. https://doi.org/10.1002/nme.6155

Chen HZ, Shen ZC, Wang L, Tian YH (2023) Probabilistic analysis of skirted foundations under combined loading in soils modelled by non-stationary random fields. Ocean Eng 272:113791. https://doi.org/10.1016/j.oceaneng.2023.113791

Chib S, Greenberg E (1995) Understanding the Metropolis-Hastings algorithm. Am Stat 49:327–335. https://doi.org/10.2307/2684568

Ching JY, Phoon KK (2019) Constructing site-specific multivariate probability distribution model using Bayesian machine learning. J Eng Mech 145:04018126. https://doi.org/10.1061/(ASCE)EM.1943-7889.0001537

Doan NS, Dang PV, Huh J et al (2022) Efficient approach for calibration of load and resistance factors in the limit state design of a breakwater foundation. Ocean Eng 251:111170. https://doi.org/10.1016/j.oceaneng.2022.111170

Dostert P, Efendiev Y, Hou TY (2008) Multiscale finite element methods for stochastic porous media flow equations and application to uncertainty quantification. Comput Methods Appl Mech Eng 197:3445–3455. https://doi.org/10.1016/j.cma.2008.02.030

Eldred M, Burkardt J (2009) Comparison of non-intrusive polynomial chaos and stochastic collocation methods for uncertainty quantification. In: 47th AIAA Aerospace Sciences Meeting including The New Horizons Forum and Aerospace Exposition. American Institute of Aeronautics and Astronautics, Orlando, FL, AIAA 2009–976. https://doi.org/10.2514/6.2009-976

Elkhatib S, Randolph MF (2005) The effect of interface friction on the performance of drag-in plate anchors. In: Gourvenec S, Cassidy M (eds) Frontiers in offshore geotechnics: ISFOG 2005. Taylor & Francis, London, pp 171–177

Elkhatib S (2005) The behaviour of drag-in plate anchors in soft cohesive soils. PhD thesis, The University of Western Australia, Perth

Feinberg J, Langtangen HP (2015) Chaospy: an open source tool for designing methods of uncertainty quantification. J Comput Sci 11:46–57. https://doi.org/10.1016/j.jocs.2015.08.008

Ghanem R (1999) Ingredients for a general purpose stochastic finite elements implementation. Comput Methods Appl Mech Eng 168:19–34. https://doi.org/10.1016/S0045-7825(98)00106-6

Ghanem R, Dham S (1998) Stochastic finite element analysis for multiphase flow in heterogeneous porous media. Transp Porous Media 32:239–262. https://doi.org/10.1023/A:1006514109327

Ghanem R, Spanos PD (1991) Stochastic finite elements: a spectral approach. Springer, New York, NY. https://doi.org/10.1007/978-1-4612-3094-6

Ghanem R, Red-Horse J, Sarkar A (2000) The modal properties of a space-frame with localized system uncertainties. In: 8th ASCE Specialty Conference on Probabilistic Mechanics and Structural Reliability, University of Notre Dame, Notre Dame, IN, Paper PMC2000–269

Griffiths DV, Fenton GA (2004) Probabilistic slope stability analysis by finite elements. J Geotech Geoenviron Eng 130:507–518. https://doi.org/10.1061/(ASCE)1090-0241(2004)130:5(507)

He P, Fenton GA, Griffiths DV (2025) Probabilistic design analysis of plate anchors in spatially variable clay. Comput Geotech 177:106828. https://doi.org/10.1016/j.compgeo.2024.106828

Hwang SH, Lee JK (2025) Probabilistic stability analysis of inclined strip anchors in spatially variable clay. Mar Georesour Geotechnol 43:1796–1807. https://doi.org/10.1080/1064119X.2024.2437049

Jakeman JD, Franzelin F, Narayan A et al (2019) Polynomial chaos expansions for dependent random variables. Comput Methods Appl Mech Eng 351:643–666. https://doi.org/10.1016/j.cma.2019.03.049

Juang CH, Ching JY, Luo Z (2013) Assessing SPT-based probabilistic models for liquefaction potential evaluation: a 10-year update. Georisk Assess Manag Risk Eng Syst Geohazards 7:137–150. https://doi.org/10.1080/17499518.2013.778117

Karhunen K (1946) Zur Spektraltheorie stochastischer Prozesse. Ann Acad Sci Fenn Ser A I Math-Phys 34:1–7

Li Z, Gong W, Zhang Z, Li T (2026) An efficient active learning-based method for reliability analysis of geotechnical structures using sparse polynomial chaos expansion. Acta Geotech 21:4353–4372. https://doi.org/10.1007/s11440-026-02930-w

Loeve M (1963) Probability theory, 3rd edn. Van Nostrand, Princeton, NJ

Marzouk YM, Najm HN, Rahn LA (2007) Stochastic spectral methods for efficient Bayesian solution of inverse problems. J Comput Phys 224:561–586. https://doi.org/10.1016/j.jcp.2006.10.010

Mathelin L, Hussaini MY, Zang TA (2005) Stochastic approaches to uncertainty quantification in CFD simulations. Numer Algorithms 38:209–236. https://doi.org/10.1007/BF02810624

Medina-Cetina Z, Yousefpour N, Briaud JL (2020) Probabilistic evaluation of unknown foundations for scour susceptible bridges. J Bridge Eng 25:04020074. https://doi.org/10.1061/(ASCE)BE.1943-5592.0001569

Menaka K, Mukherjee S, Sivakumar Babu GL, Dodagoudar GR (2026) Reliability analysis of micropile-supported deep excavations using multivariate adaptive regression splines. Geotech Geol Eng 44:101. https://doi.org/10.1007/s10706-025-03612-2

Mentani A, Govoni L, Bourrier F, Zabatta R (2023) Metamodelling of the load-displacement response of offshore piles in sand. Comput Geotech 159:105490. https://doi.org/10.1016/j.compgeo.2023.105490

Mentani A, Roy A, Chow S, Kurniadi R (2025) Using PCE metamodels to analyse the uplift capacity of circular plate anchors in sand. In: Proceedings of the 5th International Symposium on Frontiers in Offshore Geotechnics (ISFOG 2025), Nantes, France

Mushtaq M, Sahoo JP (2026) Pullout resistance of plate anchors in anisotropic and non-homogeneous clay assessed using numerical limit analysis. Geotech Geol Eng 44:57. https://doi.org/10.1007/s10706-025-03575-4

Najm HN (2009) Uncertainty quantification and polynomial chaos techniques in computational fluid dynamics. Annu Rev Fluid Mech 41:35–52. https://doi.org/10.1146/annurev.fluid.010908.165248

Oberkampf WL, Roy CJ (2010) Verification and validation in scientific computing. Cambridge University Press, Cambridge

Patil A, Huard D, Fonnesbeck CJ (2010) PyMC: Bayesian stochastic modelling in Python. J Stat Softw 35:1–81

Peng M, Yin ZY (2026) New observations on the coupling effect between factors influencing the capacity of plate anchors in clay. Ocean Eng 354:124826. https://doi.org/10.1016/j.oceaneng.2026.124826

Phoon KK, Kulhawy FH (1999) Characterization of geotechnical variability. Can Geotech J 36:612–624. https://doi.org/10.1139/t99-038

Qi XH, Zhou WH (2017) An efficient probabilistic back-analysis method for braced excavations using wall deflection data at multiple points. Comput Geotech 85:186–198. https://doi.org/10.1016/j.compgeo.2016.12.032

Randolph MF, Puzrin AM (2003) Upper bound limit analysis of circular foundations on clay under general loading. Geotechnique 53:785–796. https://doi.org/10.1680/geot.2003.53.9.785

Rappel H, Beex LAA, Hale JS et al (2020) A tutorial on Bayesian inference to identify material parameters in solid mechanics. Arch Comput Methods Eng 27:361–385. https://doi.org/10.1007/s11831-018-09311-x

Reagan MT, Najm HN, Ghanem RG, Knio OM (2003) Uncertainty quantification in reacting-flow simulations through non-intrusive spectral projection. Combust Flame 132:545–555. https://doi.org/10.1016/S0010-2180(02)00503-5

Rosenblatt M (1952) Remarks on a multivariate transformation. Ann Math Stat 23:470–472. https://doi.org/10.1214/aoms/1177729394

Rumsey KN, Francom D, Gibson G et al (2026) Bayesian adaptive polynomial chaos expansions. Stat 15:e70151. https://doi.org/10.1002/sta4.70151

Sargsyan K, Safta C, Najm HN et al (2014) Dimensionality reduction for complex models via Bayesian compressive sensing. Int J Uncertain Quantif 4:63–93. https://doi.org/10.1615/Int.J.UncertaintyQuantification.2013006821

Shen ZC, Jin DL, Pan QJ et al (2020) Probabilistic analysis of strip footings on spatially variable soils with linearly increasing shear strength. Comput Geotech 126:103653. https://doi.org/10.1016/j.compgeo.2020.103653

Shen ZC, Pan QJ, Chian SC et al (2023) Probabilistic failure envelopes of strip foundations on soils with non-stationary characteristics of undrained shear strength. Geotechnique 73:716–735. https://doi.org/10.1680/jgeot.21.00169

Soize C, Ghanem R (2004) Physical systems with random uncertainties: chaos representations with arbitrary probability measure. SIAM J Sci Comput 26:395–410. https://doi.org/10.1137/S1064827503424505

Sudret B (2008) Global sensitivity analysis using polynomial chaos expansions. Reliab Eng Syst Saf 93:964–979. https://doi.org/10.1016/j.ress.2007.04.002

Suryasentana SK, Sheil BB, Stuyts B (2024) Multifidelity data fusion for the estimation of static stiffness of suction caisson foundations in layered soil. J Geotech Geoenviron Eng 150:04024066. https://doi.org/10.1061/JGGEFK.GTENG-11819

Taiebat HA, Carter JP (2000) Numerical studies of the bearing capacity of shallow foundations on cohesive soil subjected

to combined loading. Geotechnique 50:409–418. https://doi.org/10.1680/geot.2000.50.4.409
Tibshirani R (1996) Regression shrinkage and selection via the lasso. J R Stat Soc Ser B 58:267–288. https://doi.org/10.1111/j.2517-6161.1996.tb02080.x
Tom JG, O'Loughlin CD, White DJ (2025) Reliability of dynamically embedded anchors in soft clay. Geotechnique 75:939–952. https://doi.org/10.1680/jgeot.24.00065
Tran DT, Shiau J, Keawsawasvong S, Jamsawang P (2025) Developing failure envelopes of strip anchors under combined V-H-M loadings using FELA and ADABoost models. Ocean Eng 320:120305. https://doi.org/10.1016/j.oceaneng.2025.120305
Tuminaro RS, Phipps ET, Miller CW, Elman HC (2011) Assessment of collocation and Galerkin approaches to linear diffusion equations with random data. Int J Uncertain Quantif 1:19–33. https://doi.org/10.1615/Int.J.UncertaintyQuantification.v1.i1.20
Vanmarcke EH (1977) Probabilistic modeling of soil profiles. J Geotech Eng Div 103:1227–1246. https://doi.org/10.1061/AJGEB6.0000517
Vichai K, Tran DT, Keawsawasvong S, Jamsawang P (2025) Soft-computing for 3D failure envelope of rectangular skirt foundations in heterogeneous clays. Geotech Geol Eng 43:132. https://doi.org/10.1007/s10706-025-03096-0
Vilares I, Kording K (2011) Bayesian models: the structure of the world, uncertainty, behavior, and the brain. Ann N Y Acad Sci 1224:22–39. https://doi.org/10.1111/j.1749-6632.2011.05965.x
Wang D, Hu Y, Randolph MF (2010) Three-dimensional large deformation finite-element analysis of plate anchors in uniform clay. J Geotech Geoenviron Eng 136:355–365. https://doi.org/10.1061/(ASCE)GT.1943-5606.0000210
Wang Y, Cao ZJ, Li DQ (2016) Bayesian perspective on geotechnical variability and site characterization. Eng Geol 203:117–125. https://doi.org/10.1016/j.enggeo.2015.08.017
Weisz-Patrault D, Sakout S, Ehrlacher A (2021) Energetic upscaling strategy for grain growth. II: probabilistic macroscopic model identified by Bayesian techniques. Acta Mater 210:116805. https://doi.org/10.1016/j.actamat.2021.116805
Wiener N (1938) The homogeneous chaos. Am J Math 60:897–936. https://doi.org/10.2307/2371268
Xiu D, Karniadakis GE (2002) The Wiener-Askey polynomial chaos for stochastic differential equations. SIAM J Sci Comput 24:619–644. https://doi.org/10.1137/S1064827501387826
Yang J, Zhang D, Lu Z (2004) Stochastic analysis of saturated–unsaturated flow in heterogeneous media by combining Karhunen-Loeve expansion and perturbation method. J Hydrol 294:18–38. https://doi.org/10.1016/j.jhydrol.2003.10.023
Yang M, Murff JD, Aubeny CP (2010) Undrained capacity of plate anchors under general loading. J Geotech Geoenviron Eng 136:1383–1393. https://doi.org/10.1061/(ASCE)GT.1943-5606.0000343
Yousefpour N, Downie S, Walker S, Perkins N, Dikanski H (2021) Machine learning solutions for bridge scour forecast based on monitoring data. Transp Res Rec J Transp Res Board. https://doi.org/10.1177/03611981211012693
Yousefpour N (2013) Comparative deterministic and probabilistic modeling in geotechnics: applications to stabilization of organic soils, determination of unknown foundations for bridge scour, and one-dimensional diffusion processes. PhD thesis, Texas A&M University, College Station, TX
Zhang J, Tang WH, Zhang LM (2010) Efficient probabilistic back-analysis of slope stability model parameters. J Geotech Geoenviron Eng 136:99–109. https://doi.org/10.1061/(ASCE)GT.1943-5606.0000205
Zhang J, Tang WH, Zhang LM, Huang HW (2012) Characterising geotechnical model uncertainty by hybrid Markov chain Monte Carlo simulation. Comput Geotech 43:26–36. https://doi.org/10.1016/j.compgeo.2012.02.002
Zhou WH, Yin ZY, Yuen KV (2021) Practice of Bayesian probability theory in geotechnical engineering, 2nd edn. Springer Singapore, Singapore

Publisher's Note Springer Nature remains neutral with regard to jurisdictional claims in published maps and institutional affiliations.